

A Scale-Free Analysis of Magnetic Holes in the Solar Wind

by

M. L. Stevens

B.A., Cornell University (2002)

Submitted to the Department of Physics
in partial fulfillment of the requirements for the degree of

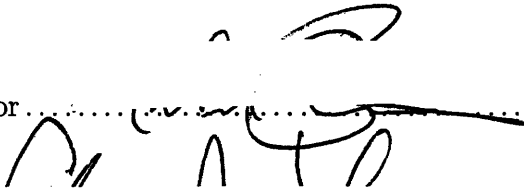
Master of Science

at the

MASSACHUSETTS INSTITUTE OF TECHNOLOGY

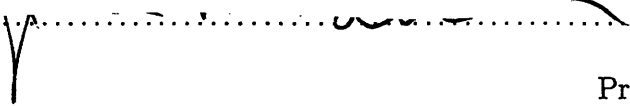
September 2006

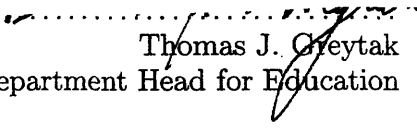
© 2006 Massachusetts Institute of Technology, all rights reserved.

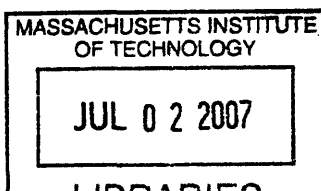
Signature of Author.....

Department of Physics
6 September 2006

Certified by.....

Alan J. Lazarus
Senior Lecturer
Thesis Supervisor

Certified by.....

John W. Belcher
Professor of Physics
Reader

Accepted by.....

Thomas J. Greytak
Associate Department Head for Education



ARCHIVES

A Scale-Free Analysis of Magnetic Holes in the Solar Wind

by

M. L. Stevens

Submitted to the Department of Physics
on 6 September 2006, in partial fulfillment of the
requirements for the degree of
Master of Science

Abstract

Magnetic holes are isolated intervals of depleted interplanetary magnetic field (IMF) strength on timescales of several seconds to several hours. These intervals have been seen as often as several times per day in the ecliptic and at high heliospheric latitudes from 1 AU to 5.4 AU. We present a scale-free statistical technique for identifying magnetic holes and evaluating their significance relative to turbulent fluctuations in the solar wind. We apply this technique in a comprehensive search for magnetic holes in the Wind and ACE magnetometer data streams through 2004. Using magnetic field and ion measurements on the Wind spacecraft, we present the first statistical study of magnetic hole plasma signatures on the kinetic scale and we present a comparison of magnetic holes as kinetic and microscale phenomena. Magnetic holes are shown to be pressure-balanced structures with similar properties on all scales. Temperature anisotropy measurements are combined with magnetic field measurements to give direct evidence that the mirror-mode instability in the solar wind is a likely source of magnetic holes. Two-satellite correlations between ACE and Wind indicate that magnetic holes are stationary with respect to the solar wind and elongated along the IMF.

Thesis Supervisor: Alan J. Lazarus
Title: Senior Lecturer

Reader: John W. Belcher
Title: Professor of Physics

Acknowledgments

This work was done at the Massachusetts Institute of Technology between Fall of 2003 and Fall of 2006 under the supervision of Dr. Alan Lazarus, Dr. Justin Kasper, and Professor John Belcher. I would like to thank them for their contributions and guidance. This work was made possible by funding from Wind Sun-Earth Connections Missions Operations and Data Analysis (MO&DA) and supported by NASA grant NRA-02-OSS-01.

Contents

1 Background	7
1.1 Summary of Previous Research	7
1.2 Theory.....	14
1.2.1 Magnetic Holes: The Model of Burlaga and Lemaire	14
2 Data Sources	17
2.1 Wind	18
2.2 ACE.....	19
3 Methods	20
3.1 Formulation of the Problem.....	20
3.1.1 Scaling.....	20
3.1.2 Isolation and Nesting	22
3.1.3 The Significance Value	22
3.1.4 Implementation.....	25
3.2 Background Characterization	26
4 Results and Discussion	30

4.1	The Magnetic Hole Database: Magnetic Signatures	30
4.2	Observations with Two Spacecraft.....	33
4.3	Plasma Signatures	37
4.4	The Plasma Beta and Kinetic Stability	39
5	Conclusions	43
	References	45
	A List of Figures and Captions.....	48

Chapter 1

Background

1.1 Summary of Previous Research

The term magnetic hole is a proxy for several plasma structures in the solar wind. The most common signature of a magnetic hole is a temporary decrease or disappearance of magnetic pressure for a period of time. Turner et al. (1977) first applied the term when they reported regions of field strength below 1 nT that occurred about 1.5 times per day over an 18-day period of observation with IMP-6. The regions were called “holes” because they seemed to occur in isolation, as discrete depressions among an otherwise uniform background field of average intensity. Some contemporary examples of this signature are shown in Figure 1 (from Zurbuchen et al., 2001). Assuming that these were signatures of structures convecting past the spacecraft at or very near the solar wind bulk speed (u_p), they were estimated to have typical sizes of about 200 proton gyroradii (R_L), and so they were deemed kinetic structures because they may be sufficiently small that the plasma cannot be treated as a fluid. Ion measurements on IMP-6 were not available at sufficiently high cadence to measure the temperatures and density within magnetic holes, so analysis focused on the relatively higher resolution magnetic field measurements. For exam-

ple, rotation of the magnetic field vector within the hole was often observed and early theoretical work focused on the magnetic hole as a pair of current sheets.

In follow-up work, magnetic holes were thought of as equilibrium structures co-moving with the bulk flow. It was hypothesized that the reduced magnetic pressure was compensated by increased plasma kinetic pressure, and that the structure was quasi-neutral. Under these assumptions, three types of self-consistent solutions to the Maxwell and Vlasov equations exist corresponding to three different rotation criteria. Firstly, the linear hole, wherein the direction of the magnetic field vector remains constant, was modeled as a region of enhanced ion pressure sandwiched between thin current sheets of opposite polarity, each normal to the corresponding magnetic field gradient. Secondly, holes with magnetic field reversal but no rotation were modeled as single pressure-balanced current sheets or groups of current sheets with the same polarity. Thirdly, holes with some magnetic field rotation were modeled as pressure-balanced structures (PBS's) having a current component parallel to the field (Burlaga & Lemaire, 1978). Fitzenreiter & Burlaga (1978) used two-satellite observations of magnetic holes to estimate the curvature of the current sheets. For four different holes, the boundary-layer current sheets were observed at both IMP-5 and IMP-6. It was thus estimated that these current sheets were planar over distances ~ 30 times the thickness at a single spacecraft, as inferred by the product of the solar wind speed and the duration of the hole passage. In each case, these holes were seen as qualitatively consistent with the models of Burlaga and Lemaire.

After the work of Burlaga and Lemaire, magnetic hole theory remained largely undeveloped for more than a decade. While the Burlaga model was self-consistent, the predictions of the theory were untested. Plasma analyzers capable of resolving charged particle densities, temperatures, and speeds at the cadence required to verify the Burlaga model would not be flown until the 1990s. The origin of magnetic holes was not speculated upon, nor was the extent of their dynamical stability. Missions such as IMP-8 continued to record the magnetic signatures of kinetic-scale holes throughout the intervening decade. At that time, magnetic decreases of the same scale were observed in the magnetosheath with ISEE 1 and 2 (Tsurutani et al., 1982). These structures were identified with the mirror mode instability, a collective mode that converts magnetic energy into thermal energy perpendicular to the field. This instability occurs in anisotropic plasmas with $T_{\perp} > T_{\parallel}$ where the plasma β (the ratio of thermal to magnetic pressure) is high. IMP-6 observations supported this theory when it was shown that the plasma depletion layer just beyond the magnetopause is usually unstable to the mirror mode (Crooker et al., 1979).

Renewed interest in magnetic holes began in 1990, when the Ulysses mission provided the unique opportunity to observe the solar wind out of the ecliptic plane at distances of 1 AU to 5.4 AU from the Sun. In a survey of magnetic holes at Ulysses from launch through the end of 1992, over four thousand events were recorded. The search criterion for this particular survey required that the magnetic field decrease to less than half the 5-minute average value (Winterhalter et al., 1994). Using SWOOPS

proton and alpha distributions and energy spectra, this study was the first to measure plasma kinetic pressure within a limited number of magnetic holes. The SWOOPS experiment provided 2-minute-average particle densities and velocity dispersion tensors every 4 to 8 minutes, an insufficient cadence for analyzing most kinetic-scale holes. Only the largest holes and holes that happened to pass Ulysses as an ion spectrum was recorded were seen by SWOOPS. Compared to the IMP, Voyager, and ISEE missions, Ulysses did not provide a superior data set in this sense. Nonetheless, the Winterhalter collaboration examined plasma data inside of and as near as possible to the magnetic holes in the survey.

Winterhalter et al. (1994) postulated a connection between linear magnetic holes, defined as holes with less than 10% rotation of the field direction, and mirror mode fluctuations, as Crooker et al. (1979) had done with isolated magnetic depletions in the magnetosheath. They were able to show that, for the few instances that particle pressures could be measured inside of the holes, there was at least some increase. They also found that the plasma in the local environment was closer to the mirror instability criterion than average, i.e. the β and the temperature anisotropy were relatively high, though in no case was the actual instability limit exceeded or matched (Winterhalter et al., 1994). In follow-up studies, the collaboration asserted that the occurrence rate of magnetic holes is correlated with stream interaction regions, and that the rate increases by a factor of ten near the ecliptic (Winterhalter et al., 2000).

Other Ulysses investigations followed to build on these results. A similar investigation selected longer duration (>2 min) Ulysses magnetic holes and found that an increase in proton anisotropy was the only bulk ion parameter correlating to the depressions in all occurrences (Fränz et al., 2000). This same study was also the first to suggest that magnetic holes exhibit scale-free behavior, with the occurrence rate varying as a power law with size over more than an order of magnitude (Fränz et al., 2000). Where Winterhalter et al. (1994) failed to demonstrate a trend in helium abundance within magnetic holes, Reisenfeld et al. (1999) were able to show that He correlates to the plasma β in pressure balanced structures (PBS's), indicating that PBS's like magnetic holes may be formed low in the solar atmosphere.

This new observational work led to theoretical efforts towards the origin of magnetic holes, some of which focused on the mirror mode instability (e.g. Baumgärtel, 1999; Fränz et al., 2000; Buti et al., 2001). Still more observational work expanded the concept of magnetic holes to include depressions on the scale of minutes to hours in duration, well beyond the kinetic scale (Chisham et al., 2000; Zurbuchen et al.; 2001, Neugebauer et al.; 2001). Zurbuchen et al. (2001) made a careful distinction between kinetic-scale magnetic holes and microscale (~ 36 s to ~ 1 hour) magnetic holes, hypothesizing that the latter are magnetohydrodynamic (MHD) structures likely formed in magnetic reconnection events in the lower corona, whereas the former should not be expected to be stable in the fluid limit.

Working in the MHD fluid limit, Baumgärtel (1997, 1999) gave two possible models of magnetic holes. Each was based on solitary wave solutions to the Derivative Nonlinear Schroedinger (DNLS) equation as applied to MHD waves (cf. Kennel et al., 1988). The first such solution predicted that magnetic holes could be mixed slow-mode/Alfvénic solitons. The second modeled magnetic holes as solitons formed by Alfvén waves propagating at wide angles relative to the magnetic field. Both models were based on 1-dimensional hybrid simulations, wherein electrons are treated as a fully isothermal fluid and ions are treated as particles-in-cells (e.g. Winske and LeCroy, 1985). In a debate that ensued between Baumgärtel (1999) and Buti (2001), Buti claimed that since the DNLS only applies to 1st order perturbations, it cannot account for stability against density fluctuations typical of the solar wind. Buti also contended that the DNLS equation is not valid for propagation at large angles to the field (Buti, 2001). Baumgärtel, in turn, cast doubt on the mirror mode hypothesis, showing that singular magnetic depressions are not typical of mirror instability saturation (Baumgärtel, 2003).

Similar MHD simulations by Buti and collaborators showed that large-amplitude Alfvén wave packets propagating at very large angles ($\sim 80^\circ$) to the magnetic field can evolve into magnetic holes similar to those observed with Ulysses (Buti et al., 2001). They showed that these holes would exhibit kinetic pressure balance. Although formation rates do depend on proton thermal anisotropy in their model, they also showed that anisotropy would not be a strict requirement for hole formation.

Tsurutani et al. (2002) proposed a second Alfvénic mechanism wherein wave pressure gradients driven by phase-steepening accelerate energetic ions in the lower solar atmosphere. These energetic ions in turn create magnetic holes by a diamagnetic effect.

At present, though the convecting PBS model for magnetic holes observed at 1 AU is generally accepted, no single process has been accepted as the mechanism for magnetic hole formation at a source region closer to the Sun. The subcategories introduced by theory (anisotropic vs. isotropic, kinetic-scale vs. microscale) have not yet been differentiated in observations. It had not been shown that magnetic holes on the scale originally defined are indeed pressure balanced or stationary because plasma measurements have generally been too slow and multi-satellite observations too rare. Furthermore, a consistent criterion had not been applied to magnetic hole identification. Though magnetic holes are pervasive in the solar wind, the number of holes observed in any given study had seldom been large enough to analyze their properties from a statistical perspective. Perhaps because of the limited availability, different projects have applied ad hoc criteria in different ways so as to get the most out of their data sets. This has hindered quantitative comparisons between different studies. It has also hindered our ability to quantitatively analyze the limitations of each.

The following questions may be regarded as unresolved:

1. What is the internal plasma structure of kinetic magnetic holes?

2. Are magnetic holes stable and/or stationary? Is the Burlaga PBS model correct?
3. What is the generation mechanism? What is the point of origin?
4. How do they scale? Are kinetic-scale and microscale holes the same?

1.2 Theory

1.2.1 Magnetic Holes: The Model of Burlaga and Lemaire

The following is a summary of the theoretical model of Burlaga, Lemaire, Turner, and others, as in the early papers Burlaga & Lemaire (1978) and Turner et al. (1977).

Assume that the direction of the solar wind magnetic field remains constant, pointing in the \hat{x} direction. Consider planar variations in \vec{B} such that $\vec{B} = B(x, z)\hat{x}$. Let the magnetic hole be elongated in the field direction, such that local to measurement we can write $\vec{B} \approx B(z)\hat{x}$. Let the magnetic field $B(z)$ transition smoothly from the background value B_0 to some B' over a transition region with width dl and then back to B_0 symmetrically at some point further upstream. Ampere's Law requires a current density in the transition regions

$$\mu_0 \vec{J} = \nabla \times \vec{B} = \frac{dB_x}{dz} \hat{y}.$$

The boundaries are a pair of oppositely-oriented current sheets with flows perpendicular to both \vec{B} and \hat{z} . Inside of the magnetic hole, $\vec{B} = B'\hat{x}$ is constant

and $|J| = 0$. Burlaga and Lemaire make the adiabatic approximation, $dl \gg R_L$, where R_L is the proton gyroradius, to decompose this current into gradient-drift and diamagnetic components. The gradient drift current is given by

$$J_D = \frac{-P_{\perp}}{B^2} \frac{dB}{dz}$$

where P_{\perp} is the perpendicular kinetic pressure, assuming a bimaxwellian distribution of thermal velocities for all species. The magnetization current is given by

$$J_M = -\frac{d}{dz} \left(\frac{P_{\perp}}{B} \right).$$

Assuming that the ions and electrons are in thermal equilibrium, the thermal velocity of electrons in the hole far exceeds the thermal velocity of ions. Burlaga and Lemaire require an electrostatic field at the boundary $\vec{E} = E(z)\hat{z}$ to maintain quasi-neutrality between the ions and the relatively mobile electrons along the magnetic field gradient. This field does not create a current, however, since electrons and protons experience an $\vec{E} \times \vec{B}$ drift in the same direction under its influence. Setting $\mu_0(\vec{J}_D + \vec{J}_M) = \nabla \times \vec{B}$ demonstrates that

$$\frac{B^2}{2\mu_0} + P_{\perp} = \text{const.}$$

Thus equilibrium is maintained across the boundary by an increase in perpendicular particle pressure, via either accumulation of particles or perpendicular heating.

The presence of a steady-state electric field at the boundary necessitates a charge separation at the boundary. The scale of charge separation in a quasi-neutral plasma sets the scale of the electric field, which must be self-consistent with the scale of the magnetic field boundary itself. In any kinetic pressure enhancement, an excess of positive charges accrues on the sparse side of the transition region. This results from the larger gyroradius of the ions compared with the gyroradius of the electrons—ions with guiding centers outside of the hole will tend to penetrate further before being reflected. In the Burlaga model, this mechanism sets the transition region scale size: $dl \sim R_L$.

Chapter 2

Data Sources

An ideal data set to answer these questions is one with magnetometer and plasma data at sufficiently high time resolutions to make many measurements within each magnetic hole. Temperature and pressure anisotropy measurements are necessary to confirm or refute many of the origin hypotheses. Measurements of each hole from two or more satellites in conjunction would illuminate the morphology, stability, and perhaps the motion of these objects relative to the bulk flow. In this study, magnetic field and ion data from the Wind spacecraft is the primary source (Ogilvie & Parks, 1996). Magnetic field data from the Advanced Composition Explorer (ACE), launched in 1997, provides a secondary source of magnetic hole observations (Stone et al., 1998). It was possible over some periods to measure the magnetic signatures of the same magnetic hole with both spacecraft.

This study is restricted to the steady solar wind. Periods where Wind was on the night side of the magnetopause were not considered. Periods associated with heliospheric current sheet crossings, coronal mass ejections, and interplanetary shocks were also omitted.

2.1 Wind

The Wind satellite was launched on November 1, 1994 as part of the ISTP program in order to provide a complete set of plasma, energetic particle, and magnetic field data streams for investigations of magnetospheric processes and basic plasma processes in the near-Earth solar wind (Ogilvie & Parks, 1996). Over the course of the mission, the spacecraft has followed a variety of orbital patterns, including extended periods in a halo orbit near the Earth-Sun L1 point and several distant prograde orbits out as far as $\sim 350 R_E$ in X_{GSE} . In all, the satellite has spent about 95% of the mission observing in the solar wind at 1 AU near the Earth and within seven degrees of the heliographic equatorial plane.

The Wind Magnetic Field Instrument (MFI) is a suite of two triaxial fluxgate magnetometers providing wide dynamic range at cadences of up to 12 vectors per second (Lepping et al., 1995). For this study, we have used the 3-second (one rotation of the Wind spacecraft) resolution data made publicly available on the web by the MFI team at <http://lepmfi.gsfc.nasa.gov/>. The Wind 3-D Plasma and Energetic Particle Investigation (3DP) produces low-energy ion spectra via a set of ion electrostatic analyzers (PESA) that sweep a 3eV to 30keV energy range 32 or 64 times for every Wind spin period. The ion density, velocity, pressure tensor, and heat flux are computed onboard and returned also at a 3-second cadence, i.e. once per revolution (Gloeckler et al., 1995). The 3DP team has made these data publicly available at <http://sprg.ssl.berkeley.edu/wind3dp/>.

2.2 ACE

The ACE magnetometer (MAG) was the flight spare for Wind, and is identical to the MFI experiment in most respects (Stone et al., 1998). At present, the quality of magnetic field measurements is assured only in the 16-second resolution Level 2 format. This resolution is sufficient for matching most kinetic scale magnetic holes that occur at both spacecraft. ACE itself is in orbit about the Earth-Sun L1 point, $220 R_E$ upstream of Earth. The ACE solar wind electron proton and alpha monitor (SWEPAM) is an electrostatic analyzer similar to PESA, operating at 0.26 to 36 keV (McComas et al., 1997). SWEPAM, which transmits plasma data every 64 seconds, can provide proton moments for some magnetic holes with relatively long duration. Level 2 SWEPAM data have also been obtained from the Web, at <http://www.srl.caltech.edu/ACE>.

Chapter 3

Methods

3.1 Formulation of the Problem

We have compiled a database of magnetic holes based on a criterion we believe to be as general as possible while adhering to the conceptual definition of Turner et al. (1997). In order to address the questions set out in Chapter 1, the search extends beyond the kinetic scale and into the micro-scale. We use the conventions of Chapter 1, where B_0 and B' refer to the magnetic field in the background and inside of the magnetic hole, respectively.

3.1.1 Scaling

It is natural to parameterize a magnetic hole signature in terms of its depth, $dB = B_0 - B'$, and its duration or length, dt . In previous studies that have approached the problem of searching for magnetic holes systematically, most have defined simple criteria based on dB . Some have required a minimum field inside of the hole, such as $B' < 1\text{nT}$ (e.g. Turner et al. 1977). Others have required a relative drop of an arbitrary magnitude, such as $dB/B_0 \gtrsim 0.9$. (e.g. Winterhalter et al. 1994). Implicit in each of these rules is that the background field, B_0 , is averaged over a window of some fixed size. The arbitrary minimum field, magnitude, and window size are

all sources of selection bias. Criteria like these also don't make a direct distinction between isolated and solitary structures.

It is of prime importance to choose a criterion that maximizes our magnetic hole database without introducing selection biases. In particular, our strategy for identifying the holes does not impose an absolute length or depth scale on our study. We follow the example of Lin et al. (1995), who realized that the magnetic field need not approach zero for a structure to have all the physical characteristics of a magnetic hole. Shallow ($dB/B_0 \lesssim 0.2$) magnetic decreases ought not to be excluded from study. We see no reason to restrict the magnetic holes by definition to the near total dropouts that had been required in previous studies (e.g. Turner et al., 1977, Winterhalter et al., 1994). Instead, we follow in the footsteps of Fränz et al. (2000), who scaled the depth of magnetic depressions in context by comparing them to the local variance of the magnetic field. Unlike Fränz et al., however, who defined local according to a sliding 300-second window, we define a neighborhood for each hole based on the scale of the hole itself. Our criterion is a function of both dB and dt , where dB is compared to the variance on a window that scales as dt . In this way, no arbitrary scales are introduced in either parameter.

To obtain as complete a list as possible, we accept or reject potential magnetic holes based on their resolvability relative to the local turbulent solar wind. With this strategy, one can avoid selection bias as long as one can adequately characterize the noisy fields and other structures in the background. When the background cannot

be characterized, potential magnetic holes found there were not included in the data set

3.1.2 Isolation and Nesting

The magnetic holes of Turner et al. (1977) were single depressions bounded by field gradients far greater than any those of any fluctuations inside of the hole or nearby. It is our objective to follow this definition closely, but we must specify a quantitative definition of a single, discrete magnetic hole. Some studies have labeled quasi-periodic trains of magnetic field depressions as magnetic holes (e.g. Winterhalter et al., 1994), and others have modeled large magnetic holes as compound objects composed of many smaller magnetic holes (e.g. Chisham et al., 2000). In order to include shallow magnetic holes in our data set, it is also necessary to distinguish between nested magnetic holes- small magnetic holes that are embedded in larger, shallow magnetic holes. We show in the next section how compound and closely-spaced magnetic holes can be naturally grouped according to the (dB, dt) parameterization.

3.1.3 The Significance Value

Consider a time series of magnetometer data with a cadence of one measurement every r seconds. On this series, choose a segment, T , centered at some element t , containing an arbitrary number of elements, n_T . The duration of this segment is $dt = r \cdot n_T$. Also choose a neighborhood, W , centered on T such that $n_W = (2s + 1) \cdot dt$

where s is some integer. We define the significance value for this segment, q_T , as follows:

$$q_T \equiv \frac{\langle |B| \rangle_{W \cap T} - \langle |B| \rangle_T}{\sigma_{W \cap T}}$$

This score represents the magnitude of the potential magnetic hole represented by the elements of T . It is the difference between the average field on T and the local average field, in units of the standard deviation of the local field. A high value of q_T indicates that the magnetic field within the region of interest is significantly lower than the local neighborhood. If T is chosen such that its boundaries coincide with the boundaries of a magnetic hole, q_T is maximized. If T contains no magnetic holes (or other magnetic signatures), q_T is generally between +1 and -1, approaching zero with sufficiently large n_T . Given a suitable choice of s , this definition provides us with a statistical measure of the significance of a magnetic field depression that can be applied on all scales. The choice of s will be discussed in Section 3.2.

By calculating the significance value at every data point (t, B) on all neighborhoods centered at that point, we can derive a map $q(t, dt)$ having maxima corresponding to the best-fit times and durations of possible magnetic holes. This is illustrated in Figure 2, which shows the significance values of a 6-minute data selection calculated out to a maximum hole duration of 5 minutes. There are two

pronounced maxima on this plot, corresponding to the two magnetic hole candidates with $(t, dt) = (7945, 12)$ and $(8067, 21)$ seconds.

Figure 2 also illustrates some common attributes of the q mapping. Each maximum is found near the convergence of two diagonal wakes, bounding a triangular region in the (t, dt) space where q exceeds the background level. This region spans all neighborhoods that contain the magnetic hole candidate. From right to left, this region encompasses neighborhoods that contain all or part of the hole candidate but are displaced from its center. Vertically, the region includes neighborhoods that are larger than the hole candidate, or that include only part of the hole. When two magnetic hole candidates are close together, these wakes intersect for neighborhoods that encompass both, as in Figure 2 at $(t, dt) = (8960, 192)$ seconds.

In practice, a single magnetic hole may be the source of an arbitrary number of local maxima in $q(t, dt)$. This is attributable to random fluctuations of the field inside of the hole and near the boundaries. Overlapping wakes can occur for nearby holes, multiple maxima in a single hole, or hierarchies of nested holes. We say that holes are nested if one hole includes the other over its entire range in t but the two are separately resolvable on different scales, dt . We say that holes are adjacent if they overlap one another in time but are separately resolvable. For a given set of local maxima, then, one must decide which peaks in q are associated and which peaks can be resolved as separate structures. Following the convention for peak detection algorithms, we require that two peaks in $q(t, dt)$ be separated by at least their width

at half of the maximum value to be separately resolved. The peak width is calculated in both dimensions: in t to distinguish nearby holes and in dt to distinguish nested holes.

3.1.4 Implementation

To identify magnetic holes on all scales, $q(t, dt)$ must be calculated for the full range of available (t, dt) . The time resolution of the Wind and ACE magnetometers sets the lower bound for dt , and the duration of the longest observed magnetic holes (~ 5 hr) is the upper bound. The computational challenge in this approach is to calculate the first two statistical moments of a time series n elements long on neighborhoods of all possible scales spanning three orders of magnitude. Taking a brute force approach, this would be an $O(n^2)$ computation.

We developed an algorithm that divides the magnetic field data into periods of a few hours, a span determined by computational resources, and calculates a vector of moments $\langle |B| \rangle_{dt}$ and $\langle B^2 \rangle_{dt}$ for all dt up to the order of the data period itself. As it calculates these moments, it builds composite matrices of these vectors over that time span. We also make use of common factorizations in order to avoid redundant calculations and streamline the algorithm to $O(n \log n)$. Multiple passes are made at different resolutions in order to sample the full range of scales.

Once these matrices are calculated for a given data period, $q(t, dt)$ is also computed and an algorithm is called to identify the peaks and group regions of en-

hanced $q(t, dt)$ accordingly. This algorithm first identifies local maxima and then recursively explores the adjacent points in the (t, dt) -space to associate each region of elevated q to the proper peak. It then identifies the half-maximum region for each peak and regroups according to the rules we described in Section 3.3. The remaining fully-resolved peaks are considered to be magnetic hole candidates. A list of the times, durations, and magnitudes $(t_{max}, dt_{max}, q_{max})$ of these candidates is compiled. For the candidate to be called a magnetic hole, the peak value, q_{max} , must exceed a threshold value, q_0 . The selection of q_0 is discussed in next section.

3.2 Background Characterization

Since we intend for our search to be fully independent of an imposed scale, it is convenient that the primary sources of magnetic fluctuations in the solar wind are scale-free processes (Goldstein et al., 1995). We have targeted the undisturbed solar wind for this study because it is relatively easy to characterize. The steady solar wind at 1 AU is in a state of well-developed turbulent flow, i.e. wave energy is being continuously transferred from long wavelength injection processes through a cascade of ever shorter wavelengths and eventually to dissipation at high frequencies. The steady-state distribution of wave power in the solar wind takes the form of a broken power law. The distribution at larger scales corresponds to the injection of wave power by processes such as shocks, stream interactions, the relaxation of beams, and solar events. This region is relatively flat, with a typical spectral in-

dex of -1 (Goldstein et al., 1995). The next region, often called the inertial range, resembles the incompressible fluid turbulence of Kolmogorov with a spectral index around $-5/3$ (Goldstein et al., 1995). The dissipation range at higher frequencies is steeper still. The power spectral density of magnetic fluctuations in the quiescent solar wind over central region, which is the timescale of interest to this study, is shown in Figure 3. All of the magnetic holes detected in this study fall in the inertial range, though the smallest holes do approach the spectral break that separates the inertial and dissipative ranges.

We assume that magnetic holes are exceptional events, and not turbulent structures intrinsic to the continuous mixing of the quiescent solar wind. In order to model the solar wind and account for turbulence, we generate random data that imitates the fluctuations in its distribution function and its power spectrum. It has been shown that, for sufficiently large time series, the probability distribution function (PDF) of magnetic field fluctuations is roughly Gaussian (e.g. Tu and Marsch, 1994). We take the following steps to generate synthetic data with these properties:

1. The real data in the region of interest are Fourier-transformed. A linear least squares fit is used to fit the inertial domain to a power law and determine the spectral index.

2. A synthetic time series of Gaussian-distributed random numbers is generated using the Box-Muller method (cf. Press et al., 1999).

3. The synthetic time series is Fourier-transformed and multiplied in the Fourier domain by the power law fit of step 1.

4. The series is transformed back to the time domain.

The resulting time series is normally distributed, but with a spectral index matching that of the region of interest.

The magnetic hole search algorithm was applied to real data and to synthetic data generated in this way. Magnetic hole detections in the model data are taken to be false positives: random turbulent fluctuations that happen to imitate magnetic hole signatures. The frequency of false positives in the model data provides a baseline for the real magnetic hole search. It also provides us with a way to choose optimum values for the free parameters of the algorithm, s and q_0 .

The parameter s dictates how many times smaller a magnetic hole must be than the neighborhood it is compared to. For large values of s , a given magnetic hole must be highly isolated, as any large fluctuations (such as another hole) in the neighborhood of the hole will increase σ_W and thus decrease q_{max} for the hole. We call s the isolation factor.

The parameter q_0 sets a minimum hole magnitude. It is not useful or tractable to record q_{max} down to arbitrary size- the vast majority of the peaks would be statistically insignificant. We call q_0 the cutoff.

The cutoff and the isolation factor are chosen in order to maximize the number of events while minimizing the relative frequency of false positives generated

in the model data. Let N be the number of magnetic holes found in some segment of the real data and let \tilde{N} be the number of magnetic holes found in the model data for that segment, then the certainty is defined simply as $(N - \tilde{N})/N$. A plot of $(N - \tilde{N})/N$ for different values of s and q_0 is shown in Figure 4. A locus of points is apparent where about 3% or less of the holes are false positives. We choose $q_0 = 7$ and $s = 4$, which provides the highest N and the lowest s on this locus. The highest possible N maximizes our data set, and the lowest s , reduces computational requirements because it requires less overlap when scanning for the largest magnetic holes in a given pass. Henceforth, the neighborhood or the local region of a magnetic hole will refer to an interval with $s = 4$, excluding the hole itself.

Chapter 4

Results and Discussion

The search program found 2074 magnetic holes at Wind with $q_{max} \geq 7$ over the decade from 1994 to 2004. These holes are all well-resolved, isolated, and accompanied by a correlated ion signatures. Figures 5 and 6 show two representative examples of magnetic hole cross sections measured at Wind.

4.1 The Magnetic Hole Database: Magnetic Signatures

Over the ranges applicable to this study, Figure 7 illustrates that there is no characteristic size or magnitude for magnetic holes. In the absence of scaling biases we find that the distributions of size and scaled magnitude q_{max} are well-fit by power law trends, indicating that the scale-free search method was appropriate. We also find that magnetic holes are typically linear, with no apparent preference towards total annihilation of the field. We find that field annihilation events like the magnetic holes of previous studies are actually part of a continuum over the decade from 1994 to 2004. The average occurrence rate of one per 1.75 days is somewhat lower than the 1.5 events per day observed by Turner continuum of magnetic decreases of all depths.

The search program found magnetic holes at Wind with an average occurrence rate of one every 1.75 days. This rate is somewhat lower than the 1.5 events per day observed by Turner and Burlaga (1977) or the 5.3 events per day recorded by Winter-

halter et al. in the high-latitude solar wind (1994). The discrepancy is a direct result of the selectivity of the study. The rate of one hole per 1.5 days is appropriate to the 97% certainty level we have required. Magnetic holes were most commonly detected near the $q_0 = 7$ cutoff, however holes with q_{max} up to and exceeding 100 were seen (see Figure 7a). Over the entire population, the relative frequency of magnetic holes at the $q_{max} \cdot \sigma$ level is well described by the following empirical power law:

$$N(q_{max}) \propto q_{max}^{(-4.16 \pm 0.09)}, \text{ with } \chi^2/dof = 0.83.$$

The typical magnetic hole magnitudes and dimensions in this study differ markedly from previous studies. The average relative drop in the magnetic field was $dB/B_0 = 0.2$, with a typical minimum field of 3.43 nT. Figure 7c shows the distribution of dB/B_0 for the entire sample. The number of holes observed is a monotonically decreasing function of the relative drop down to a drop of $dB/B_0 \sim .06$, typically about ~ 0.3 nT. Due to spacecraft charging and other sources of error that cannot be calibrated for on short timescales, the Wind MFI experiment has a typical noise level on the order of $\sim 0.1-0.2$ nT (A. Szabo, private communication). We expect the majority of magnetic holes with dB/B_0 near or below this noise threshold to escape detection. Disregarding the rollover at the noise limit, we ascertain that magnetic holes in the solar wind at 1 AU have no characteristic depth. Our finding that holes occur at a rate that is inversely proportionate to depth is in general agreement with the find-

ings of Fränz et al (2000) using the statistical “s-criterion,” which is similar to our criterion but applied to holes of specific size.

Figure 7b also shows the hole cross-sectional widths in units of the proton gyroradius (R_L), assuming that the holes are stationary in the plasma frame. In this plot, the occurrence rate is a decreasing function of width for widths above about $130 R_L$. Below this size, the number of magnetic holes appears to be an increasing function of size. An unavoidable selection bias arises, however, for magnetic holes with durations near the minimum detectable duration set by the Wind MFI resolution (3 seconds). The statistics of holes near the resolution limit are further complicated because their true widths cannot be determined to within an order of magnitude. For the statistics of hole duration, we have omitted holes shorter than 9 seconds, requiring three corroborating points to estimate the peak location in $q(t, dt)$. To quantify the selection bias, we measured the distribution of ion inertial lengths for generic 9-second periods in the solar wind, finding that the most frequent value is $61 R_L$, and the average value is $137 R_L$. We expect our selection bias to have a significant effect on the distribution at and below this range. It is most likely, then, that the rollover in Figure 7b is a result of the bias, and not an indicator of a characteristic scale. For widths $dx \gtrsim 100R_L$, the empirical distribution is again a power law:

$$N(dx) \propto dx^{(-1.73 \pm 0.07)}, \text{ with } \chi^2/dof = 0.86.$$

Whereas the result of Fränz et al. contained weak indications of the existence of a breakpoint in the range of $\sim 200\text{-}800 R_L$, our data do not support a change in the spectral index over any sub-range greater than $\sim 130 R_L$. If some change of mechanism does occur at scales below $130 R_L$, it is not detectable from the count rates alone.

We also note that rotation of the field vector inside of the hole is usually small in this sample (see Figure 7d). The most probable rotation is about 5° , and about 39% of the holes have rotations of 10° or less. There were no field-reversal structures in this sample. The noise threshold at $dB \lesssim 0.1$ nT becomes significant for rotations of about $2\text{-}3^\circ$ and below, affecting only the leftmost bin in Figure 7d. The majority of the magnetic holes in this sample are comparable to the linear holes of Burlaga and Lemaire (1978).

4.2 Observations with Two Spacecraft

When the search algorithm was applied to the ACE MAG data set from mid 1997 through 2004, it identified 743 magnetic holes. The rate of detection is about 0.16 per day, compared to the 0.18 per day rate at Wind for holes >16 seconds long. For each magnetic hole observed at ACE, the list of magnetic holes at Wind was cross-checked for events occurring within the bulk flow time interval $d\tau = \pm\tau_0$, where $\tau_0 \equiv r_{Wind-ACE}/u_p$ where u_p is the bulk flow speed of the solar wind.

None of the ACE magnetic holes were identified at Wind at the $q_{max} \geq 7$ level. We consider several possible explanations. One possible explanation is that magnetic holes are so transient that they seldom survive long enough to convect from ACE to Wind, typically about 30 minutes. This is unlikely, as large magnetic holes are often seen with sizes on the order of the spacecraft separation itself, with durations up to and exceeding 30 minutes. Another possibility is that they are stationary with respect to the Earth, which might be the case if magnetic holes were caused by the Earth's bow shock. This would contradict the limited multi-satellite observations that have been made to date. Using considerably smaller data sets, other groups have found that large magnetic holes upstream of the bow shock are convecting with the ambient solar wind (e.g. Chisham et al., 2000).

A third and more likely explanation follows from the fact that most magnetic hole observations are noise-limited. The turbulent fluctuations that form our baseline exist on applicable scales and evolve on an Alfvénic timescale, where the Alfvén speed is comparable to, but typically somewhat slower than, the bulk speed ($v_A \sim 50$ km/s, $u_p \sim 400$ km/s). The satellites observe different “cuts” of the hole, and likewise different cuts of the background. Most magnetic hole candidates are rejected for failing to meet the $q_{max} \geq 7$ criterion, so perhaps the chances of passing the test again at a later time, in a different cut, and against background fluctuations that evolve on this timescale are simply too remote.

We selected a set of time periods that sampled a wide range of ACE-Wind separations for thorough cross-correlation analysis. During this selection, Wind and ACE made a close pass as Wind approached and underwent one halo orbit around the Earth-Sun L1 point in 1998. For each upstream magnetic hole found in this period, we searched for a corroborating signature at the downstream spacecraft within the bulk flow time interval. In lieu of the $q_{max} \geq 7$ criterion at the second spacecraft, we consider strong correlation with a bona fide upstream magnetic hole to be sufficient. We define a strong correlation as having a maximum correlation coefficient over the hole neighborhood that exceeds 0.8 for some time delay $\tau < \tau_{max}$. τ_{max} is chosen to be greater than the bulk flow timescale, τ_0 , and also greater than the corotation timescale, i.e. the time it would take for a corotating structure to encounter the second spacecraft for the largest spacecraft separations in this data selection.

Two populations of correlated holes emerged on two different scales. We separated these two populations based on the convention of Burlaga et al. (1968) into kinetic and microscale events. 167 kinetic-scale ($\lesssim 150 R_L$) magnetic holes were matched, primarily when ACE was downstream of Wind. 60 ($\gtrsim 150 R_L$) microscale magnetic holes were matched. The time delays between Wind and ACE for matched kinetic-scale holes are plotted in Figure 8 as a function of spacecraft separation, with the bulk speed time delay τ_0 subtracted out. The slope of the best-fit line is less than the error of the fit. This means that, within error, the kinetic holes are convecting from one satellite to the next at the bulk flow speed. In contrast, Figure 9 shows

$\tau - \tau_0$ for the microscale holes. The white line indicates the corotation time delay and the red dashed line is the line of best fit. In this case, the time delay matches the corotation delay to within the error of the fit.

These two populations are probably not indicative of two different types or characteristic scales of magnetic holes. Instead, they imply that magnetic holes are extended along the magnetic field. We note that most of the kinetic-scale holes were matched at small separations ($\sim 10R_E$) where Wind was in slow orbit around L1 just in front of ACE. In this position, Wind and ACE were frequently aligned with respect to the plasma bulk flow (nearly parallel to \hat{x}_{GSE} , in the Geocentric Solar Ecliptic coordinate system), and typically separated by comparable distances in x_{GSE} and y_{GSE} , which may account for the scatter in Figure 8. Most of the microscale holes, by contrast, were matched at large separations ($\sim 100R_E$) where Wind was closer to Earth in x_{GSE} and significantly further from ACE in y_{GSE} . At these separations, Wind and ACE more often measure spatially separated sections of the same elongated structure than measure the same local section of a structure with any shape. For structures elongated in the field-aligned direction, the resulting time delay is the corotation delay. Larger structures are more likely to be matched in this way, as we have confirmed.

4.3 Plasma Signatures

The dynamical stability of magnetic holes depends in part on pressure equilibrium with the local plasma flow. We have found evidence for pressure balance across magnetic holes at all scales. For each magnetic hole the proton thermal pressure was calculated inside and outside of the hole. The relative change in scalar kinetic pressure, dP_i , is plotted as a function of the change in magnetic pressure, dP_B , in Figure 10. In 92% of the cases where dP_B exceeds the measurement error in P_i , the magnetic pressure decrease is compensated by a comparable proton kinetic pressure increase. Figure 5 shows an example of one such hole, where the amplitudes of ion pressure and magnetic pressure change are large but the total pressure is unperturbed. Figure 10 shows the direct correspondence between the two parameters for the entire sample, along with the line of best fit. Along the line, $dP_i \sim 0.69 \cdot dP_B$, i.e. the total ion kinetic pressure increases to compensate 69% of the magnetic pressure decrease in the magnetic hole.

Assuming quasi-neutrality, we can infer the electron contribution to the kinetic pressure were the holes to be pressure balanced structures. If the electrons were in thermal equilibrium with the ions, the electron kinetic pressure change would be equal to the ion kinetic pressure change. This limit would require $dP_i/dP_B = dP_e/dP_B = 0.5$ for dynamical stability. In general, for electron temperature T_e' inside of the hole, the electron kinetic pressure change is given by

$$dP_e \simeq a \cdot dP_i - P_i' \left(a - \frac{T_e'}{T_i'} \right)$$

where P_i' and T_i' are the ion scalar kinetic pressure and temperature inside of the hole, respectively, and $T_e = aT_i = aT_0$ outside of the hole. For holes with $dP_i/dP_B > 0.5$, as in most of our sample, the pressure balance requirement is typically consistent with preferential heating of the ions in the solar wind with $a \sim 2$.

The changes in ion temperature and density across magnetic hole boundaries are compared in Figure 11. For 87% of all cases, there is both significant heating and enhancement of proton density within the hole. The magnitudes of the density and temperature increases are both strong functions of the magnetic pressure change. Larger holes, however, generally owe more of their kinetic pressure to heating when compared to smaller holes. In shallow holes, the relative changes in temperature and density are comparable; for example when $dP_B/P_{tot} < 0.15$, we find that $dT_p/T_{p,0} \sim 1.2 \cdot dN_p/N_{p,0}$ on average. In the deepest holes, the relative heating exceeds the relative condensation; for example in the 72 cases where $dP_B/P_{tot} > 0.5$, we find that $dT_p/T_{p,0} \sim 2 \cdot dN_p/N_{p,0}$. One possible explanation for this effect would be an evolutionary process wherein ions are heated in the annihilation of magnetic energy at the creation of the hole, and then cooled again as heat diffuses out and cooler ions fall in as the magnetic field depression erodes. In such a model, the lifetime of the magnetic hole would be set by the heat diffusion timescale across the field. This model is also consistent with the high abundance of shallow magnetic holes, which

would decay more slowly since the cross-field heat diffusion rate varies as dT/B^2 (Chen, 1984).

There is evidence that the magnetic hole generation mechanism increases the ion temperature anisotropy, heating preferentially perpendicular to the field. The characteristic proton temperature anisotropy parameter inside of magnetic holes in this study is $T_{\perp}/T_{\parallel} = 0.86 \pm 0.01$, whereas the characteristic temperature anisotropy outside is 0.80 ± 0.01 . This is only an 8% effect, but it is statistically significant and appropriate when compared to the average temperature increase of $\sim 20\%$. The distribution of temperature anisotropies in and around magnetic holes is shown in Figure 12. The thermal anisotropy of the solar wind at 1 AU in general is lower, with a most probable value of 0.64. The fact that magnetic holes occur preferentially with high anisotropy supports the theory that holes are created by an ion temperature anisotropy instability such as the mirror mode.

4.4 The Plasma Beta and Kinetic Stability

We have found that magnetic holes occur preferentially when the plasma β of the solar wind (the ratio of kinetic pressure to magnetic pressure) is high. When the average ion-component of the plasma beta was calculated in the neighborhood of each magnetic hole, we found that the most common value of the ion plasma beta in these neighborhoods is 0.6, and the median value is 1.0. These values are significantly higher than those of the solar wind at 1 AU over the entire decade. In

Figure 13, we compare the full distribution of ion plasma beta in the solar wind is compared to the distribution near magnetic holes. In the figure, most of the magnetic holes in this study fall in the high-beta tail of the solar wind distribution, where the relative occurrence rate is more than ten times the occurrence rate at the peak. The occurrence rate is an increasing linear function of beta up to beta ~ 1.55 . Above 1.55, the trend appears to level off somewhat before it becomes obscured by low counts.

Instabilities driven by ion temperature anisotropy become significant in the high-beta tail of the solar wind. Protons can become resonant with the mirror-mode and ion cyclotron instabilities in the high-beta solar wind at anisotropies $T_{\perp}/T_{\parallel} > 1$. At particularly high beta ($\beta \gtrsim 5$), the mirror-mode instability is theoretically the dominant effect in a purely proton-electron plasma. In the presence of helium, this threshold may actually be somewhat lower while the ion cyclotron threshold is somewhat higher (Gary, 1993). Of these two instabilities, numerical simulations and observations in the magnetopause have shown that the nonlinear evolution of mirror mode waves can result in isolated pressure-balanced structures. We have found evidence that a significant number of magnetic holes are the remnants of nonlinear mirror-mode waves.

Figure 14 shows the proton temperature anisotropies and plasma betas for the entire magnetic hole sample. Also plotted is the stability criterion for the mirror instability. We define the instability parameter R as:

$$R \equiv \frac{T_{p,\perp}/T_{p,\parallel}}{1 + 1/\beta_{p,\perp}}, \text{ where } \beta_{p,\perp} \equiv \frac{n_p k T_{p,\perp}}{B^2/2\mu_0}.$$

When $R > 1$, the plasma is said to be unstable to the mirror-mode and shallow magnetic field depletions ($dB/B_0 \lesssim 0.1$) can be shown by linear theory to grow at an exponential rate (Gary, 1993). We note that there are 47 magnetic holes (2.3% of the population) in plasma that is unstable in this sense. Of the 47 unstable-region holes, none are shallower than $dB/B_0 = 0.1$, possibly owing to the fact that shallow holes would quickly grow until they reached the nonlinear regime where $dB \sim B$. Next, we note that deep magnetic holes occur preferentially near the instability threshold whereas shallow holes concentrate in more stable low-B regime. The color-scaling in Figure 14 shows that hole depth and proximity to the mirror threshold are correlated.

Mirror mode structures in plasma where $R < 1$ are stable on dynamical timescales owing to pressure balance. On timescales set by the coulomb collision rate and solar wind expansion, however, the plasma and magnetic field diffuse self-consistently. A point of origin ~ 1 AU, i.e. near the Sun, would be required for holes to decay significantly on these timescales before reaching Wind. This diffusion process will be the subject of future statistical work. The observations presented thus far, however, suggest a timeline where magnetic holes begin their lifetime in the $R > 1$ region and then gradually come into temperature equilibrium and isotropy as they decay. In this picture, magnetic holes would migrate from the upper-right to the lower-left of Figure 14, moving most quickly early in their lifetime and finally lin-

gering as they become very shallow and the diffusion rate decreases asymptotically. We might also speculate that as the mirror mode saturates, most holes are initially created with depths $dB/B_0 \sim 1$. Our observation that the number of magnetic holes present in the solar wind decreases with depth is consistent with this initial depth and asymptotically slowing diffusion rate.

This line of reasoning reconciles our results with the results of at least one study that restricted the magnetic hole definition to a low cutoff, i.e. $B' \leq 1nT$. These magnetic holes, such as the holes of Winterhalter et al. (1994), Turner et al. (1977), Neugebauer et al. (2001), and others, are a subset consisting only of *young* holes. These holes are near saturation, and thus should be closer to the instability threshold, on average, than the holes of this study. This is indeed the case for the Winterhalter et al. study, which found that 4% of events with $B' < 1nT$ were in actively unstable plasmas, and that most were in marginally stable plasma with $\beta > 1$ and $T_{p,\perp}/T_{p,\parallel} \sim 1$.

Chapter 5

Conclusions

We have shown that magnetic holes may be identified statistically with a scale-free and unbiased procedure. Applying this procedure to Wind and ACE data in the solar wind at 1 AU, we have demonstrated that magnetic holes exist with similar properties on length scales of ~ 10 to ~ 1000 proton gyroradii and the full range of detectable magnitudes. Using high-resolution ion data from Wind, we have analyzed the plasma properties local to and inside of magnetic holes and made the following new observations:

Internal Plasma Structure: Magnetic holes are accompanied by increases in ion kinetic pressure. Typically, both the proton density and the proton temperature are higher inside of a magnetic hole than in the local environment. The ion temperature plays a stronger role in this pressure enhancement than the density in deep magnetic holes. The ion thermal distributions inside of magnetic holes tend to have higher values of the proton temperature anisotropy $T_{p,\perp}/T_{p,\parallel}$.

Stability and Trajectory: Ion measurements inside of magnetic holes are consistent with the theory that they are pressure-balanced structures. Timing measurements between ACE and Wind for small holes show that they are stationary with respect to the solar wind.

Generation Mechanism: The occurrence rate of magnetic holes increases strongly with the plasma β and temperature anisotropy of the local environment. Deeper holes are more likely to be found in plasmas that are unstable to the mirror-mode than shallow ones. The hole depth is correlated with proximity to the instability threshold in the $(\beta, T_{\perp}/T_{\parallel})$ parameter space. It is highly likely that many magnetic holes are remnants of the mirror-mode instability.

Scaling: There is no distinction between kinetic-scale and microscale magnetic holes over the range of cross-sectional lengths from ~ 10 to ~ 1000 proton gyroradii. Timing measurements between ACE and Wind for larger holes show that they are extended along the magnetic field direction.

For future work, a similar study of electron properties in magnetic holes would make it possible to confirm the pressure balance inside and confirm the hypothesis that they are created by an ion-associated instability. Knowing more about the thermal evolution of magnetic holes could also tell us about their point of origin. To this end, relationships between the thermal properties and diffusive timescales of magnetic holes will be the subject of a future statistical study.

References

- [1] Baumgärtel, K., Soliton approach to magnetic holes, *J. Geophys. Res.*, *104*, 28295, 1999.
- [2] Baumgärtel, K., Fluid approach to mirror mode structures, *Plan. & Space Sci.*, *49*, 1239, 2001
- [3] Baumgärtel, K., K. Sauer, and E. Dubinin, Towards understanding magnetic holes: Hybrid simulations, *Geophys. Res. Let.*, *30*, SSC 4-1, 2003
- [4] Burlaga, L. F., and J. F. Lemaire, Interplanetary Magnetic Holes: Theory, *J. Geophys. Res.*, *83*, 5157, 1978.
- [5] Buti, B., B. T. Tsurutani, M. Neugebauer, and B. E. Goldstein, Generation mechanism for magnetic holes in the solar wind, *Geophys. Res. Let.*, *28*, 1355, 2001
- [6] Chen, F. F., 1984, Introduction to Plasma Physics and Controlled Fusion (2nd ed., New York: Plenum Press).
- [7] Chisham, G, S. J. Schwartz, D. Burgess, S. D. Bale, M. W. Dunlop, and C. T. Russell, Multisatellite observations of large magnetic depressions in the solar wind, *J. Geophys. Res.*, *105*, 2325, 2000.
- [8] Crooker, N. U., T. E. Eastman, and G. S. Stiles, Observations of plasma depletion in the magnetosheath at the dayside magnetopause, *J. Geophys. Res.*, *84*, 869, 1979.
- [9] Fitzenreiter, R. J., and L. F. Burlaga, Structure of Current Sheets in Magnetic Holes at 1 AU, *J. Geophys. Res.*, *83*, 5579, 1978.
- [10] Fränz, M., D. Burgess, and T. S. Horbury, Magnetic field depressions in the solar wind, *J. Geophys. Res.*, *105*, 12725, 2000.
- [11] Gary, S. P., 1993, Theory of Space Plasma Microinstabilities (New York: Cambridge University Press)
- [12] Gliem, D. C. Hamilton, T.E. Holzer, D. Hovestadt, F. M. Ipavich, E. Kirsch, R. A. Lundgren, K. W. Ogilvie, R. B. Sheldon, and B. Wilken, The solar

wind and suprathermal ion composition investigation on the Wind spacecraft, *Space Sci. Rev.*, 71, 79, 1995.

- [13] Gloeckler, G., H. Balsiger, A. Burgi, P. Bochsler, L. A. Fisk, A. B. Galvin, J. Geiss, F. Gliem, D. C. Hamilton, T.E. Holzer, D. Hovestadt, F. M. Ipavich, E. Kirsch, R. A. Lundgren, K. W. Ogilvie, R. B. Sheldon, and B. Wilken, The solar wind and suprathermal ion composition investigation on the Wind spacecraft, *Space Sci. Rev.*, 71, 79, 1995.
- [14] Goldstein, M. L., D. A. Roberts, and W. H. Matthaeus, Magnetohydrodynamic Turbulence In The Solar Wind, 1995, *Ann. Rev. Astronomy and Astrophysics*, 33, 183, 1995.
- [15] Kennel, C. F., B. Buti, T. Hada, R. Pellat, Nonlinear, dispersive, elliptically polarized Alfvén waves, *Phys. Fluids*, 31, 1949, 1988.
- [16] Lepping, R. P., M. H. Acuna, L. F. Burlaga, W. M. Farrell, J. A. Slavin, K. H. Schatten, F. Mariani, N. F. Ness, F. M. Neubauer, Y. C. Whang, J. B. Byrnes, R. S. Kennon, P. V. Panetta, J. Scheifele, and E. M. Worley, The Wind Magnetic Field Investigation, *Space Sci. Rev.*, 71, 207, 1995.
- [17] McComas, D. J., S.J. Bame, P. Barker, W. C. Feldman, J. L. Phillips, P. Riley, and J. W. Griffée, Solar Wind Electron Proton Alpha Monitor (SWEPAM) for the Advanced Composition Explorer, *Space Sci. Rev.*, 86, 563, 1998.
- [18] Neugebauer, M., B. E. Goldstein, D. Winterhalter, E. J. Smith, R. J. McDowell, and S. P. Gary, Ion distributions in large magnetic holes in the fast solar wind, *J. Geophys. Res.*, 106, 5635, 2001.
- [19] Ogilvie, K. W., and G.K. Parks, First Results from WIND Spacecraft: An Introduction, *Geophys. Res. Lett.*, 23, 1179, 1996.
- [20] Press, W.H., S. A. Teukolsky, W. T. Vetterling, and B. P. Flannery 1999, *Numerical Recipes in C: The Art of Scientific Computing* (2nd ed., New York: Cambridge University Press).
- [21] Stone, E.C., A. M. Frandsen, R. A. Mewaldt, E. R. Christian, D. Margolies, J. F. Ormes, F. Snow, The Advanced Composition Explorer, *Space Sci. Rev.*, 86, 1, 1998.

- [22] Tsurutani, B. T., E. J. Smith, R. R. Anderson, K. W. Ogilvie, J. D. Scudder, D. N. Baker, and S. J. Bame, Lion roars and nonoscillatory drift mirror waves in the magnetosheath, *J. Geophys. Res.*, *87*, 6060, 1982.
- [23] Tu, C.-Y., and E. Marsch, E., MHD structures, waves and turbulence in the solar wind: Observations and theories, *Space Sci. Rev.*, *73*, 1-2, 1995.
- [24] Turner, J. M., L. F. Burlaga, N. F. Ness, and J. F. Lemaire, Magnetic Holes in the Solar Wind, *J. Geophys. Res.*, *82*, 1921, 1977.
- [25] Winske, D. and M. M. Leroy, Hybrid simulation techniques applied to the Earth's bow shock, 1985, in Computer simulation of space plasmas (Tokyo/Dordrecht, Netherlands, Terra Scientific Publishing Co./D. Reidel Publishing Co.)
- [26] Winterhalter, D. M., M. Neugebauer, B. E. Goldstein, E. J. Smith, S. J. Bame, and A. Balogh, Ulysses field and plasma observations of magnetic holes in the solar wind and their relation to mirror-mode structures, *J. Geophys. Res.*, *99*, 23371, 1994.
- [27] Winterhalter, D. M., E. J. Smith, M. Neugebauer, B. E. Goldstein, B.T. Tsurutani, The latitudinal distribution of solar wind magnetic holes, *Geophys. Res. Lett.*, *27*, 1615, 2000.
- [28] Zurbuchen, T. H., S. Hefti, L. A. Fisk, G. Gloeckler, N. A. Schwadron, C. W. Smith, N. F. Ness, R. M. Skoug, D. J. McComas, and L. F. Burlaga, On the origin of microscale holes in the solar wind, *J. Geophys. Res.*, *106*, 16001, 2001.

Appendix A

List of Figures and Captions

Figure 1: Plasma Signature example (from Zurbuchen et al., 2001)

Examples of magnetic holes observed at ACE from Zurbuchen et. al. (2001).

Magnetic hole durations vary from seconds to hours.

Figure 2: $q(t, dt)$ for a magnetic hole.

Example of the significance value plotted over (dt, t) for a magnetic hole.

The wake features indicate neighborhoods containing but poorly fitting the hole. The maximum at $(t, dt) = (8067, 21)$ seconds indicates that the algorithm has identified a magnetic hole 21 seconds long at $t = 8067$ seconds.

Figure 3: Solar wind inertial-range turbulence with Kolmogorov spectral index

Figure 4: Relative certainty of magnetic hole detections when real data are compared to synthetic data. The plotted value is $(N - \tilde{N})/N$ as a function of cutoff and isolation factor. The upper right region of this plot is limited by infrequent detections, whereas the lower left is dominated by false positives. The pixel at $q_0 = 7$ and $(2s + 1) = 9$ optimizes certainty and count frequency.

Figure 5: Example of a kinetic-scale magnetic hole time series. This hole is linear, with enhancements in ion density, temperature, and temperature anisotropy.

The stacked pressure plot, second row from the bottom, indicates that the ion pressure increase nearly compensates the magnetic pressure decrease.

Figure 6: Example of a microscale magnetic hole time series. This hole has a small field rotation, and the ion pressure increase is attributable almost entirely to the increase in temperature. The temperature anisotropy in the hole is dramatically increased.

Figure 7: Basic histograms for the Wind magnetic hole search. Note the power-law trends in hole size and significance value.

Figure 8: Wind-ACE time delays for kinetic-scale magnetic holes in 1998. The blue line indicates the expected time delay for an extended, corotating structure. A slope of zero corresponds to the time delay expected for a localized structure that is frozen into the solar wind.

Figure 9: Wind-ACE time delays for microscale magnetic holes in 1998. The congregation of points around the corotation delay indicates that these structures are extended along the magnetic field.

Figure 10: Ion scalar kinetic pressure increase dP_i as a function of magnetic pressure decrease dP_B . Most magnetic holes demonstrate significant kinetic pressure increases.

Figure 11. Ion scalar temperature increase scatter-plotted against ion density increase in magnetic holes. Compared to the density increase, the slope of the tem-

perature increase trend is steeper and perhaps upturned, implying that the temperature plays an increasingly large role increasing magnetic hole depth.

Figure 12. Distribution of the temperature anisotropy T_{\perp}/T_{\parallel} . The temperature anisotropy in near-hole plasma tends to be somewhat greater than in the average solar wind. The anisotropy is greater still inside of magnetic holes, which is consistent with a thermal anisotropy instability.

Figure 13. Distribution of plasma β near magnetic holes and in the general solar wind at 1 AU. The magnetic hole occurrence rate increases dramatically with the plasma β before it becomes obscured by insufficient statistics.

Figure 14. Scatter plot of plasma β vs. temperature anisotropy T_{\perp}/T_{\parallel} near magnetic holes. The black curve indicates the mirror-mode instability threshold, and the color-coding corresponds to hole depth. Deeper holes appear to congregate near the instability threshold.

Figure 15. Distribution of the mirror-mode instability parameter in magnetic holes, near magnetic holes, and in the solar wind at 1 AU. The magnetic hole occurrence rate increases with the instability parameter before it is obscured by insufficient statistics. The increased value inside of holes is also indicative of the instability's action.

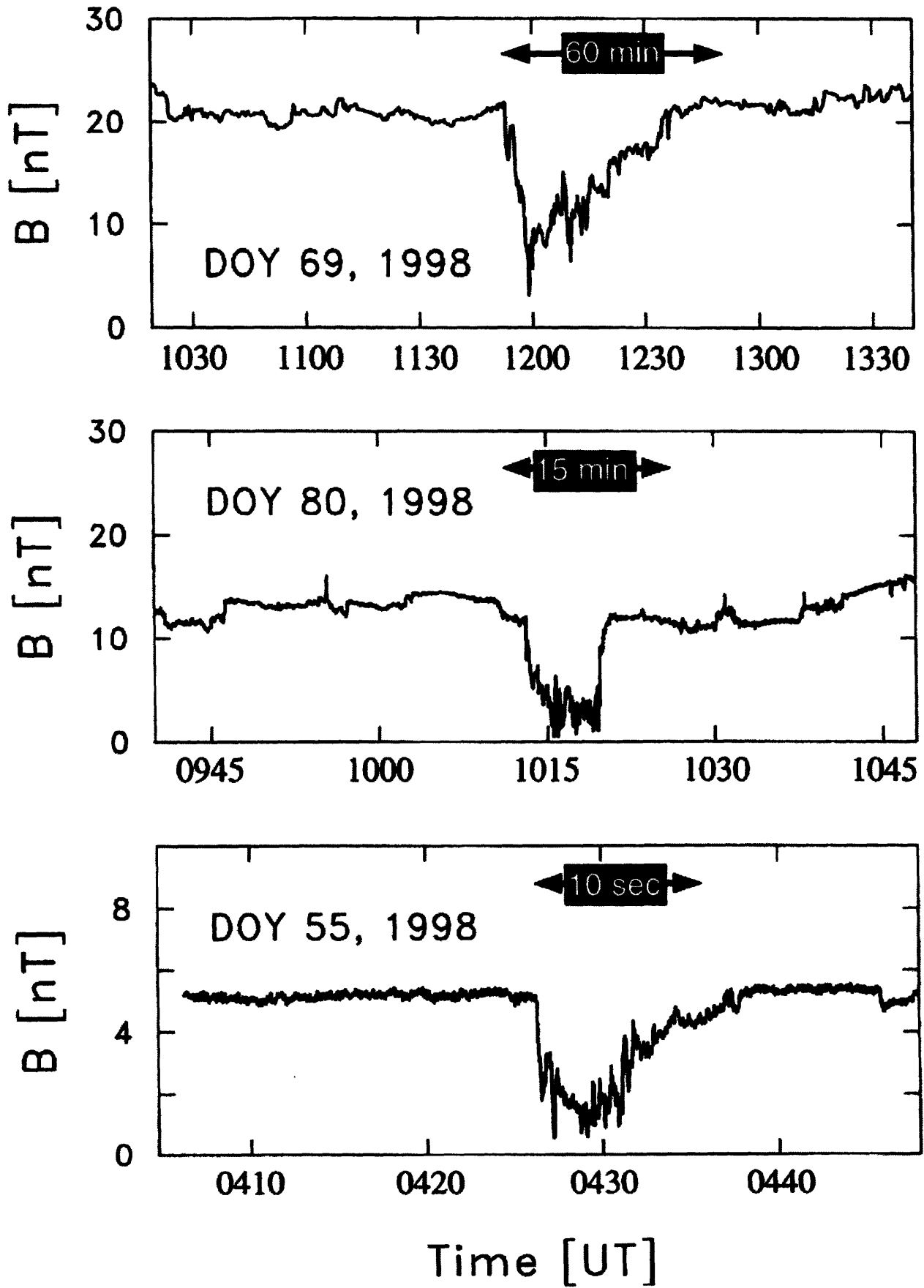


Figure 1

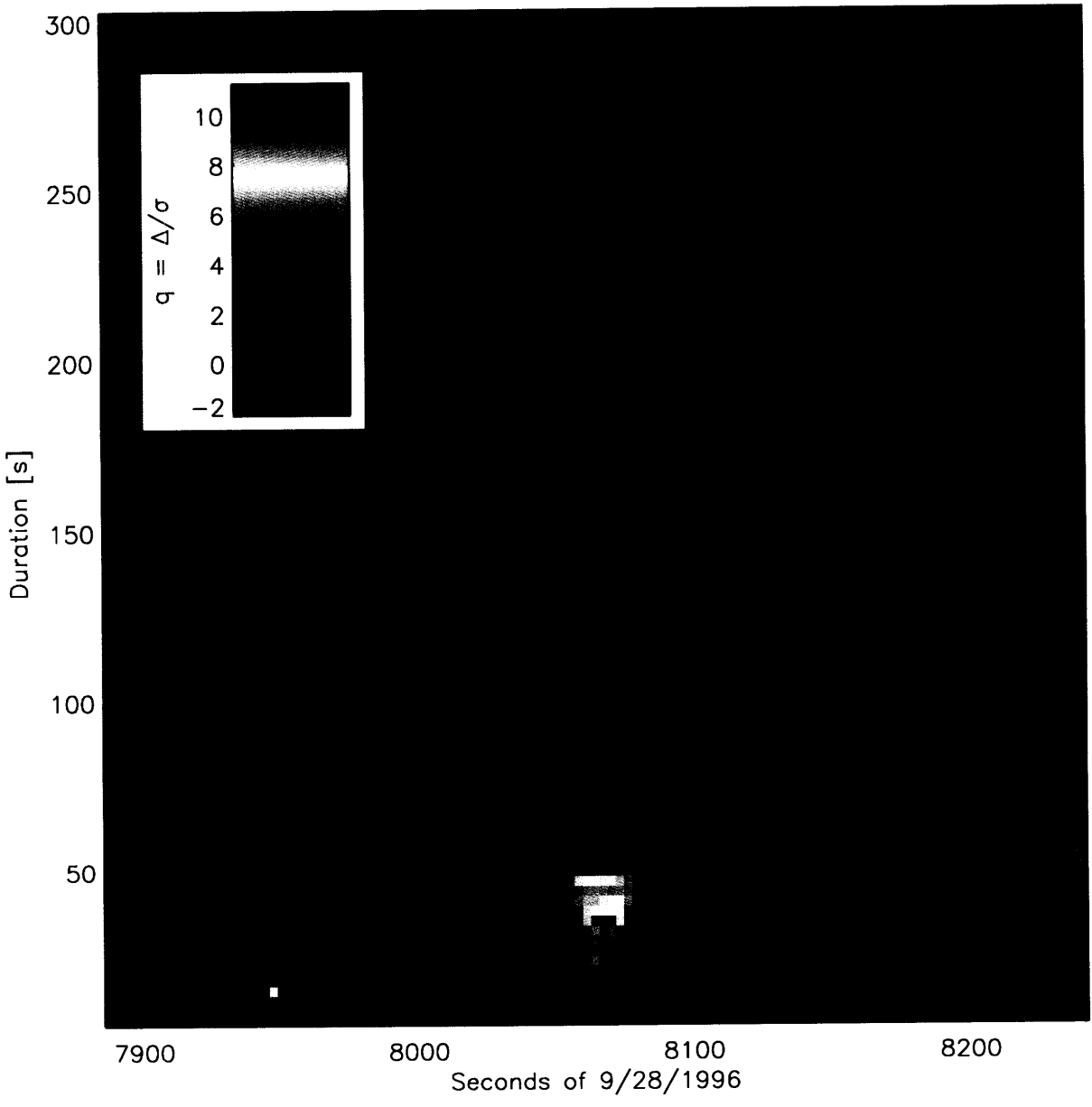
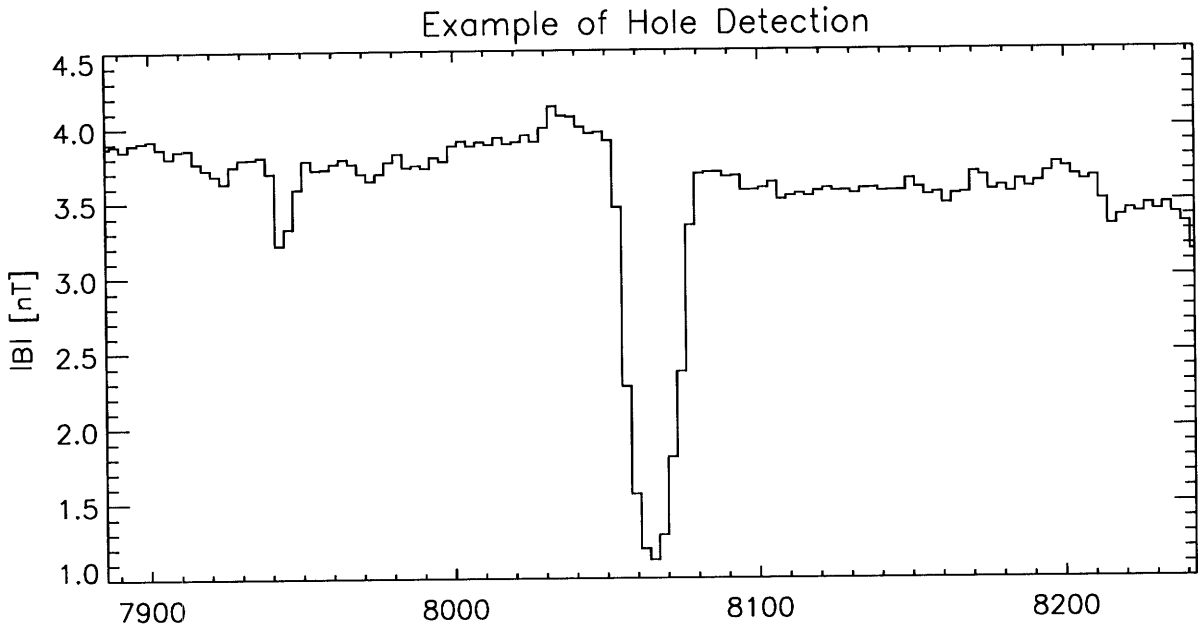


Figure 2

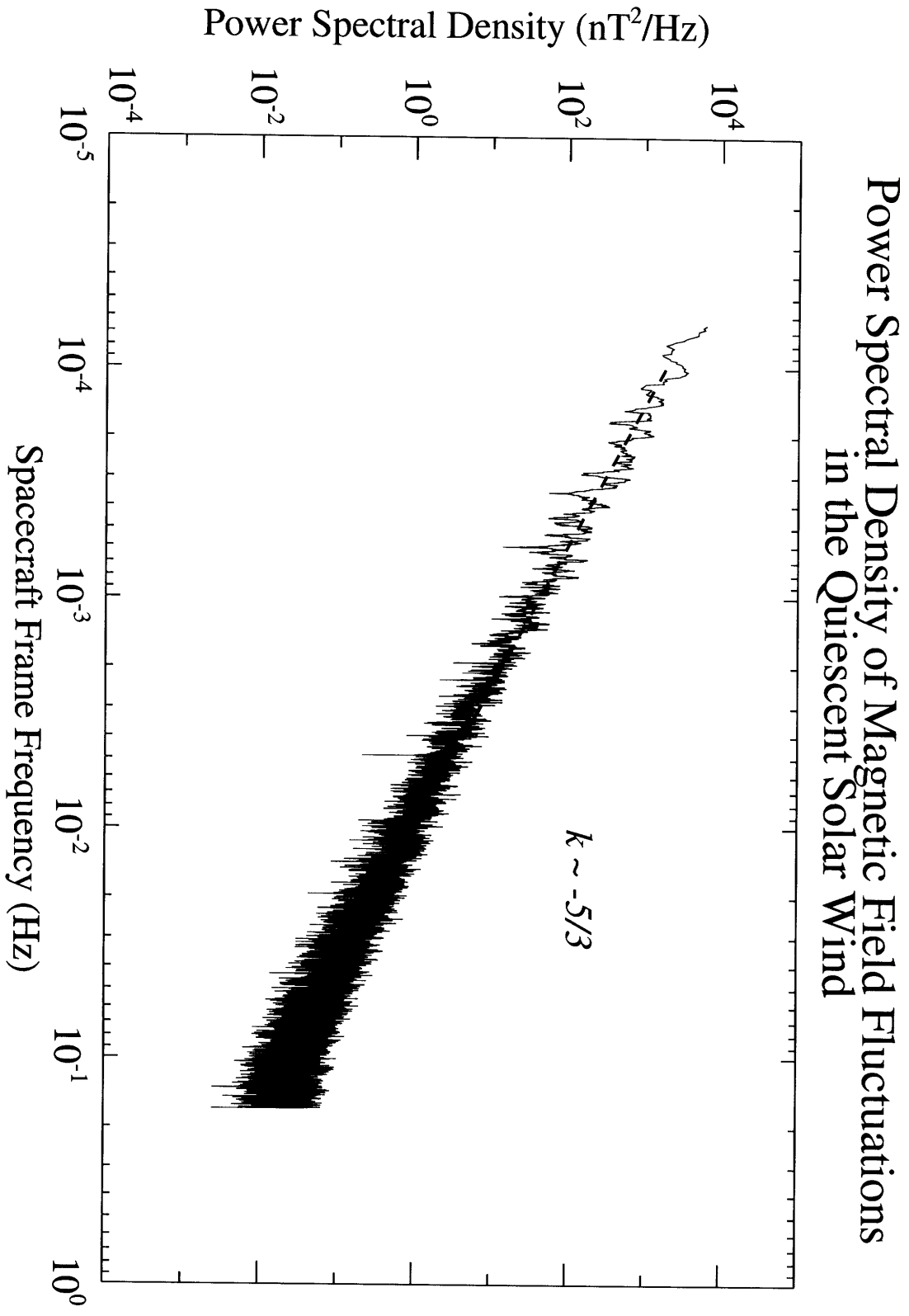


Figure 3

Certainty of Non-random MH Events

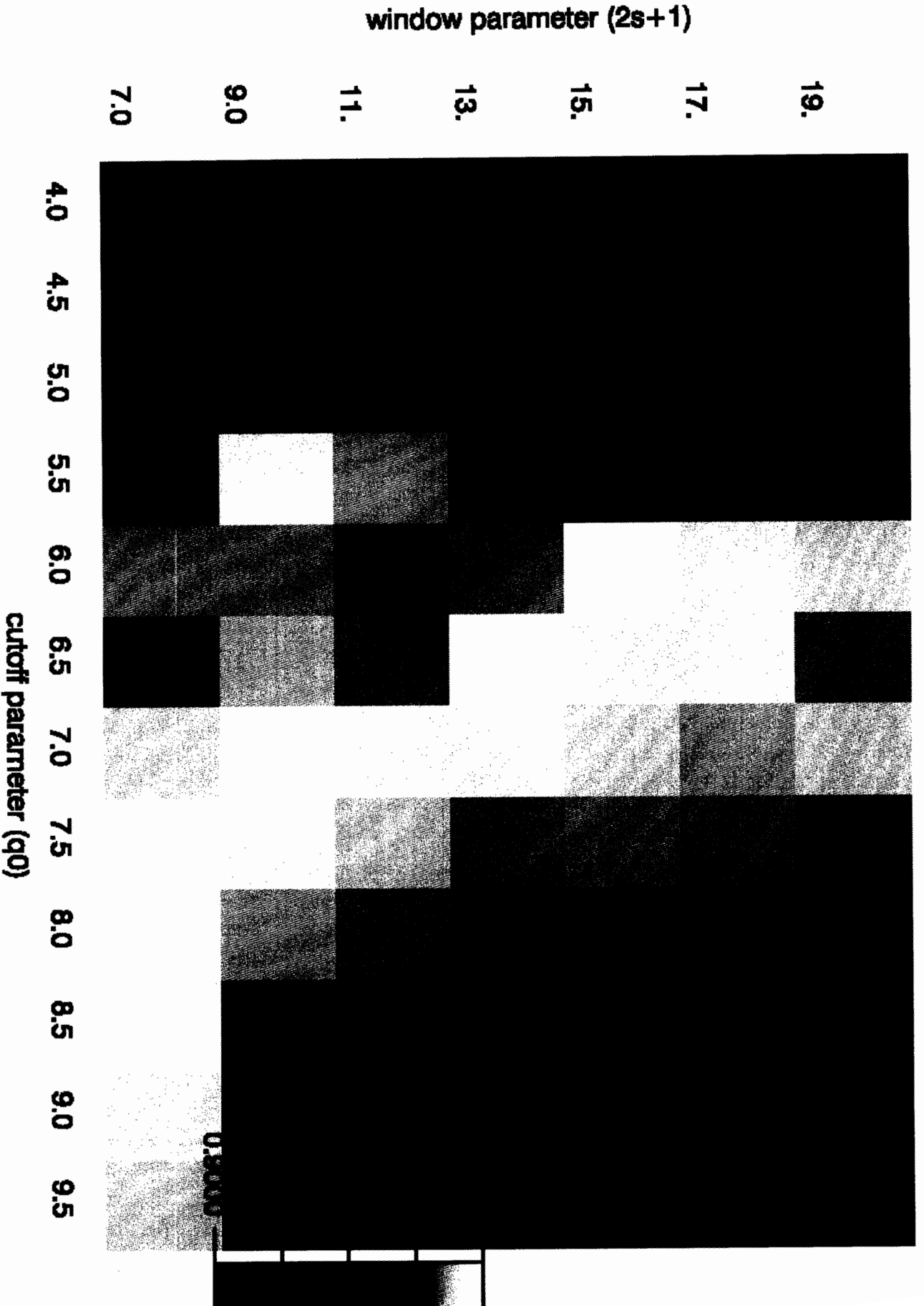


Figure 4

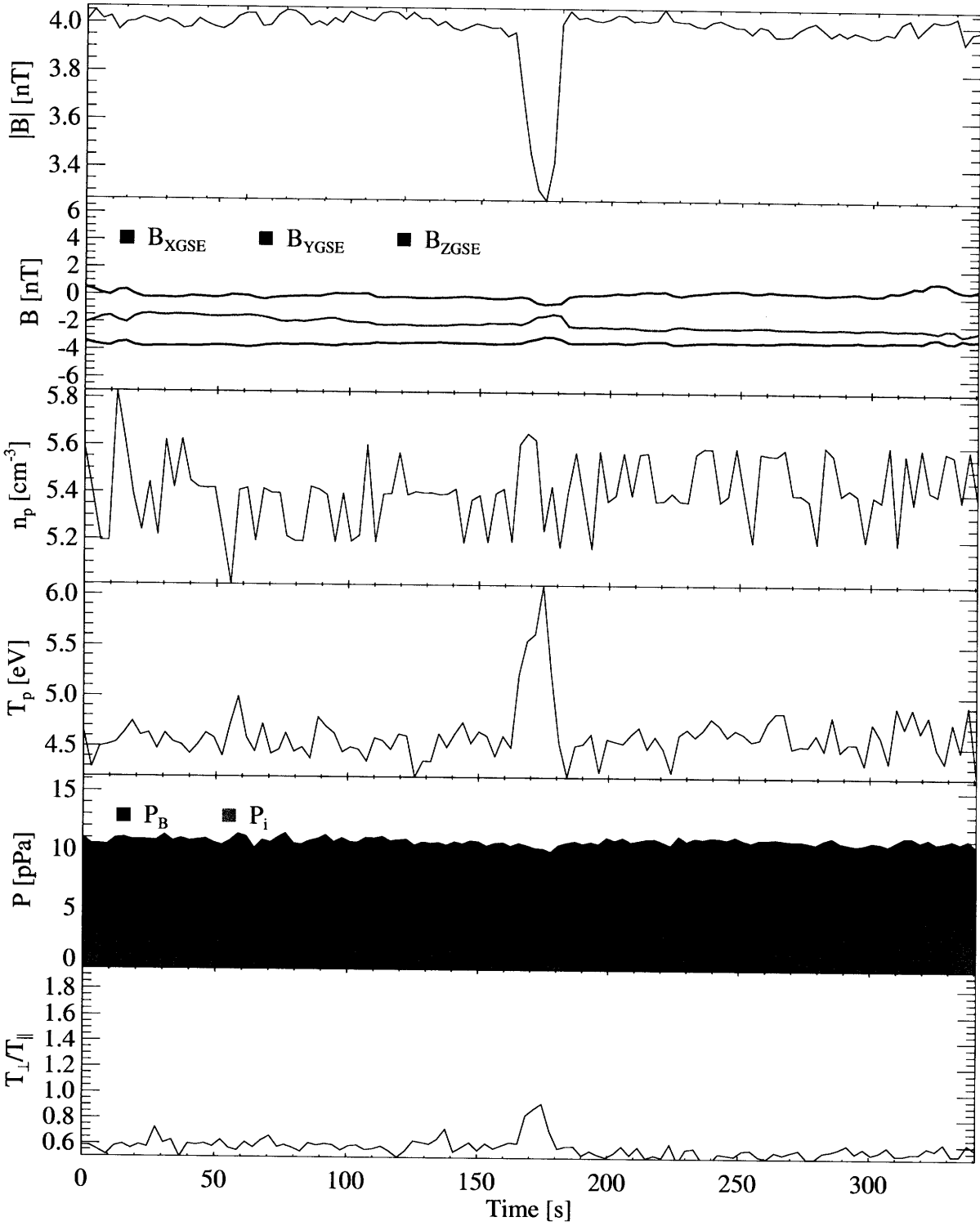


Figure 5

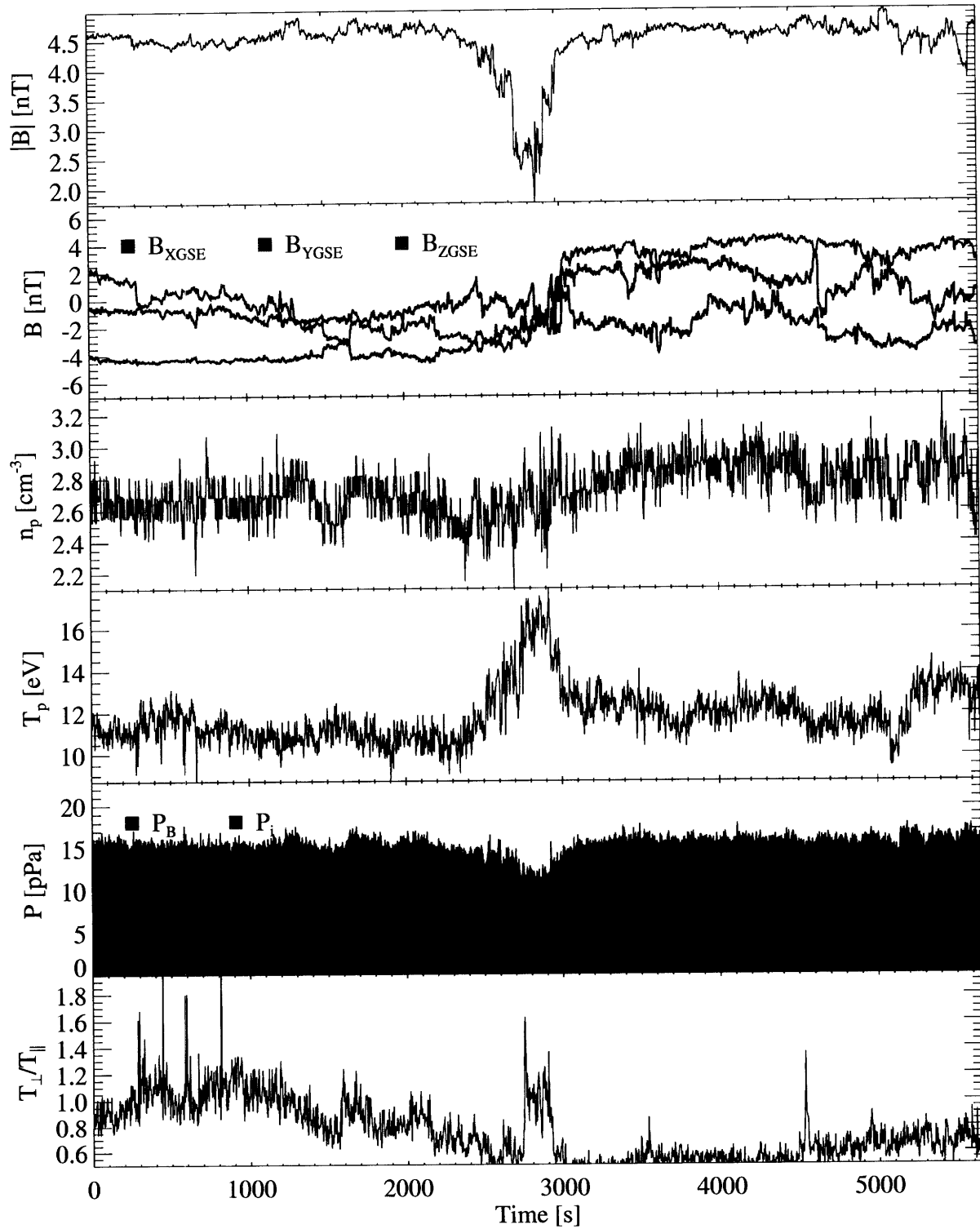


Figure 6

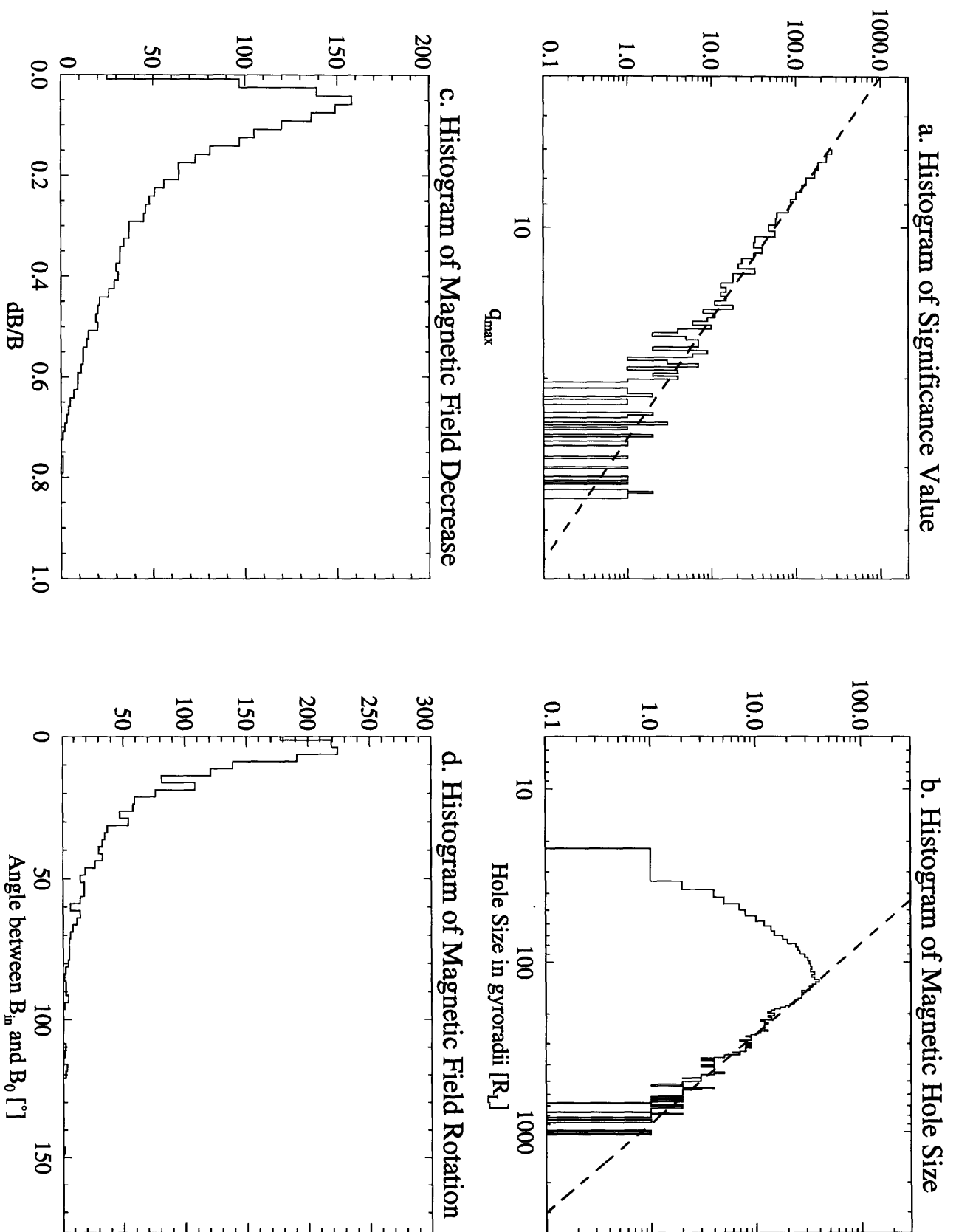


Figure 7

Wind-ACE Time Delay for Kinetic Holes

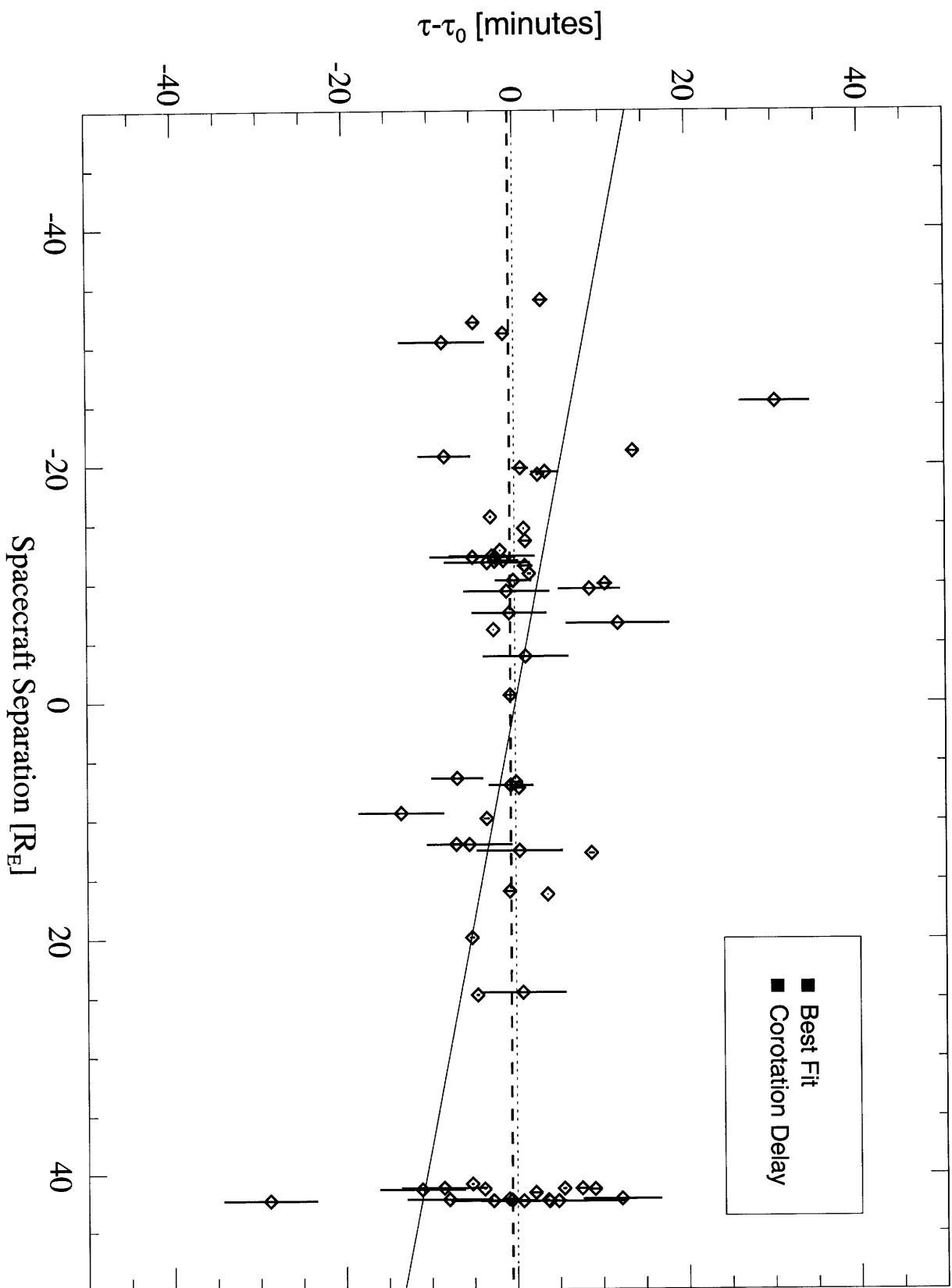


Figure 8

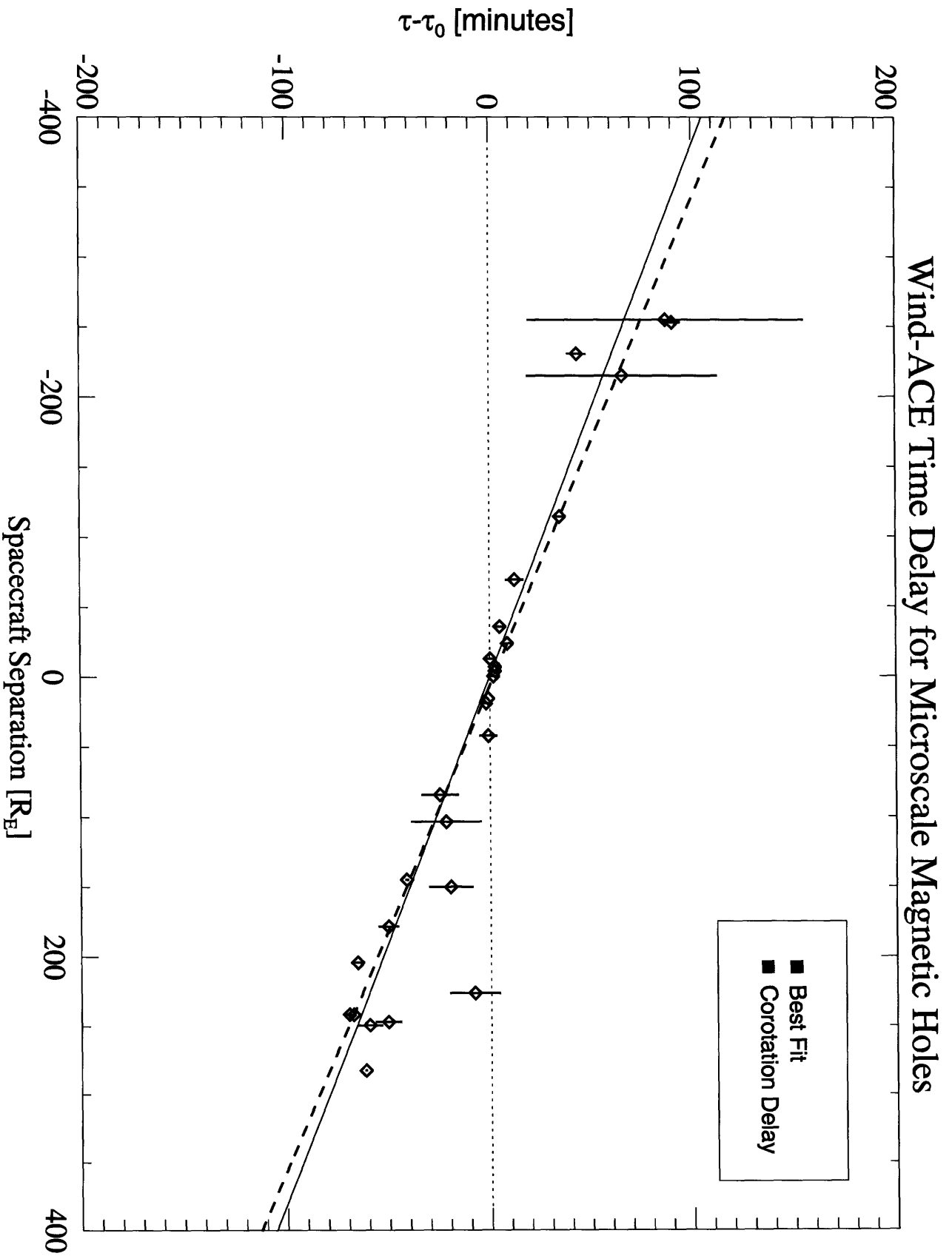


Figure 9

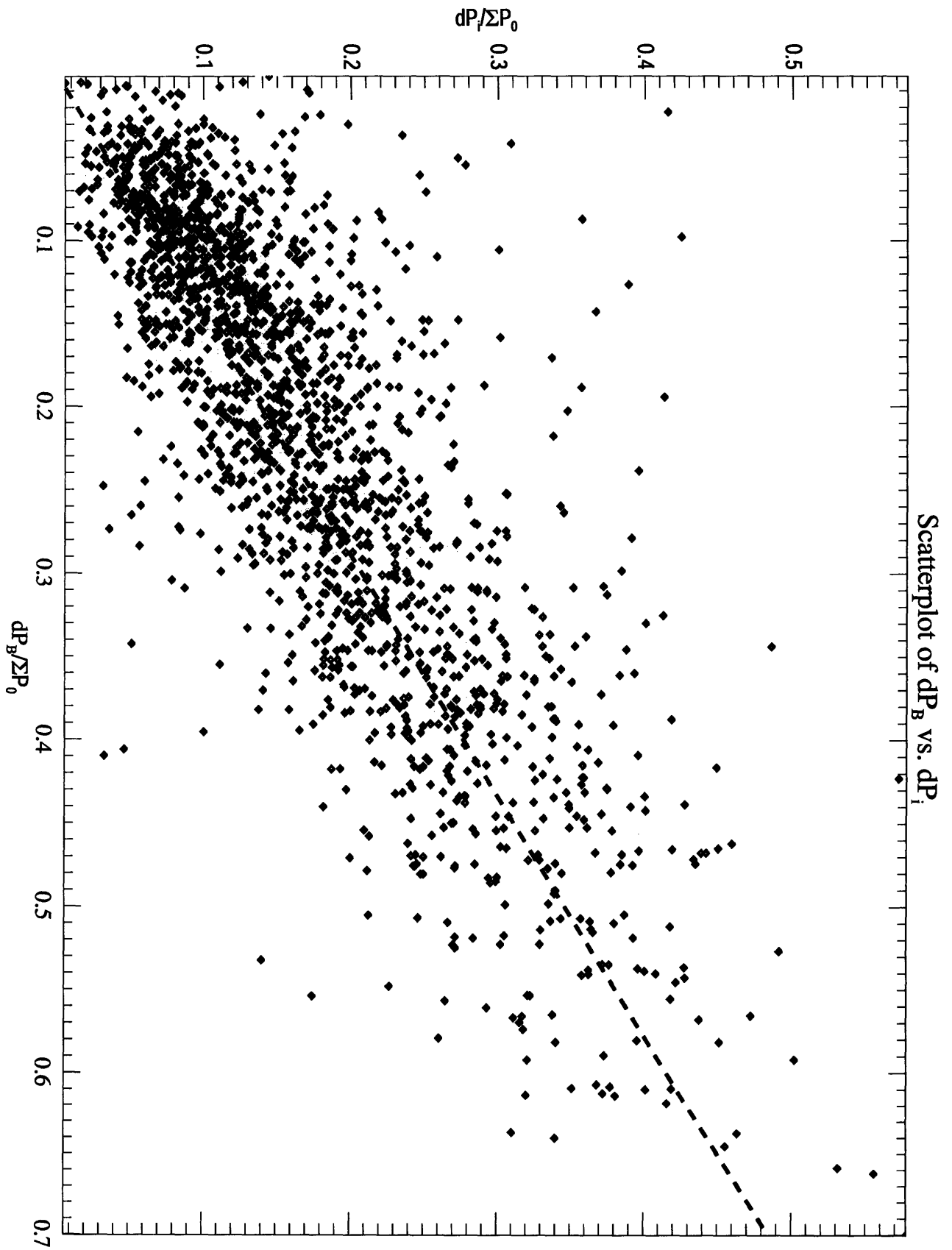


Figure 10

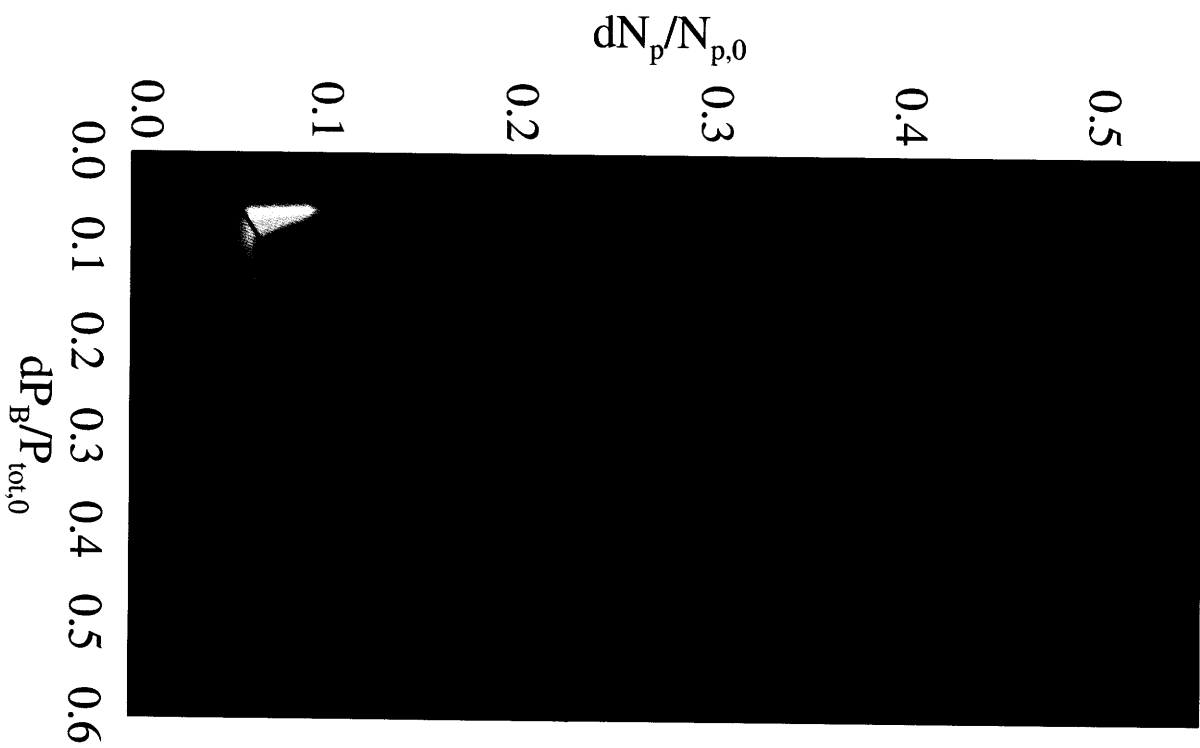
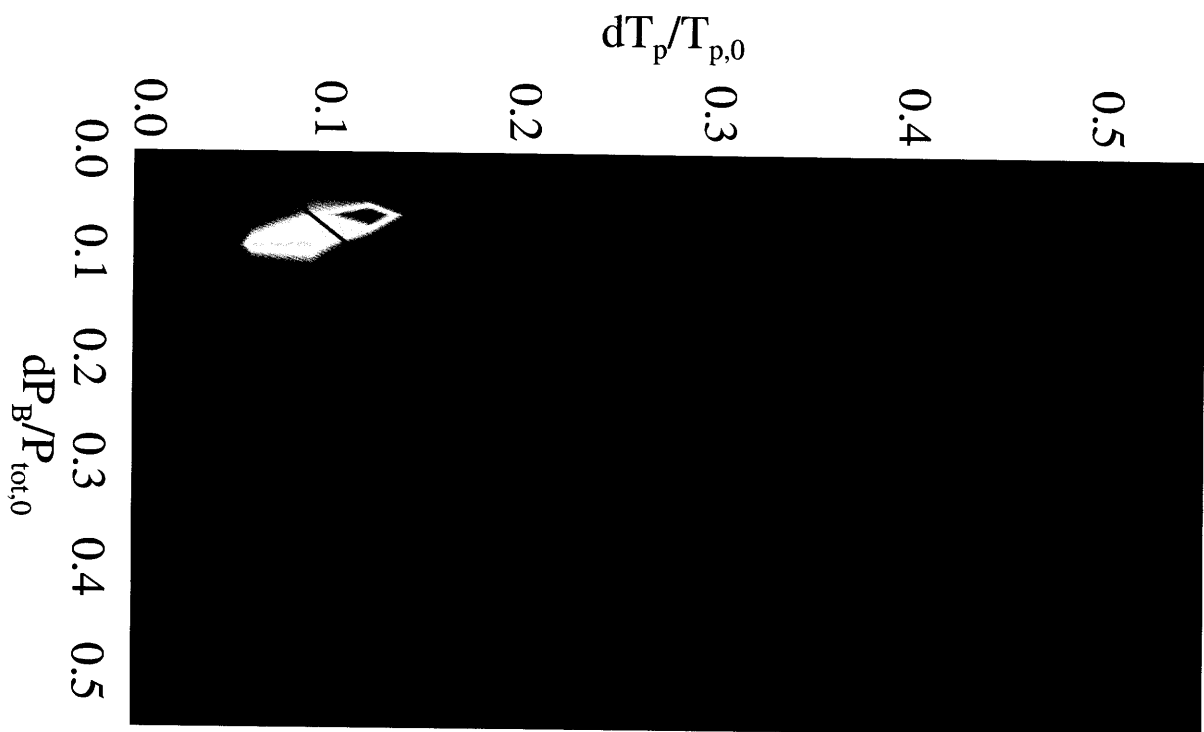


Figure 11

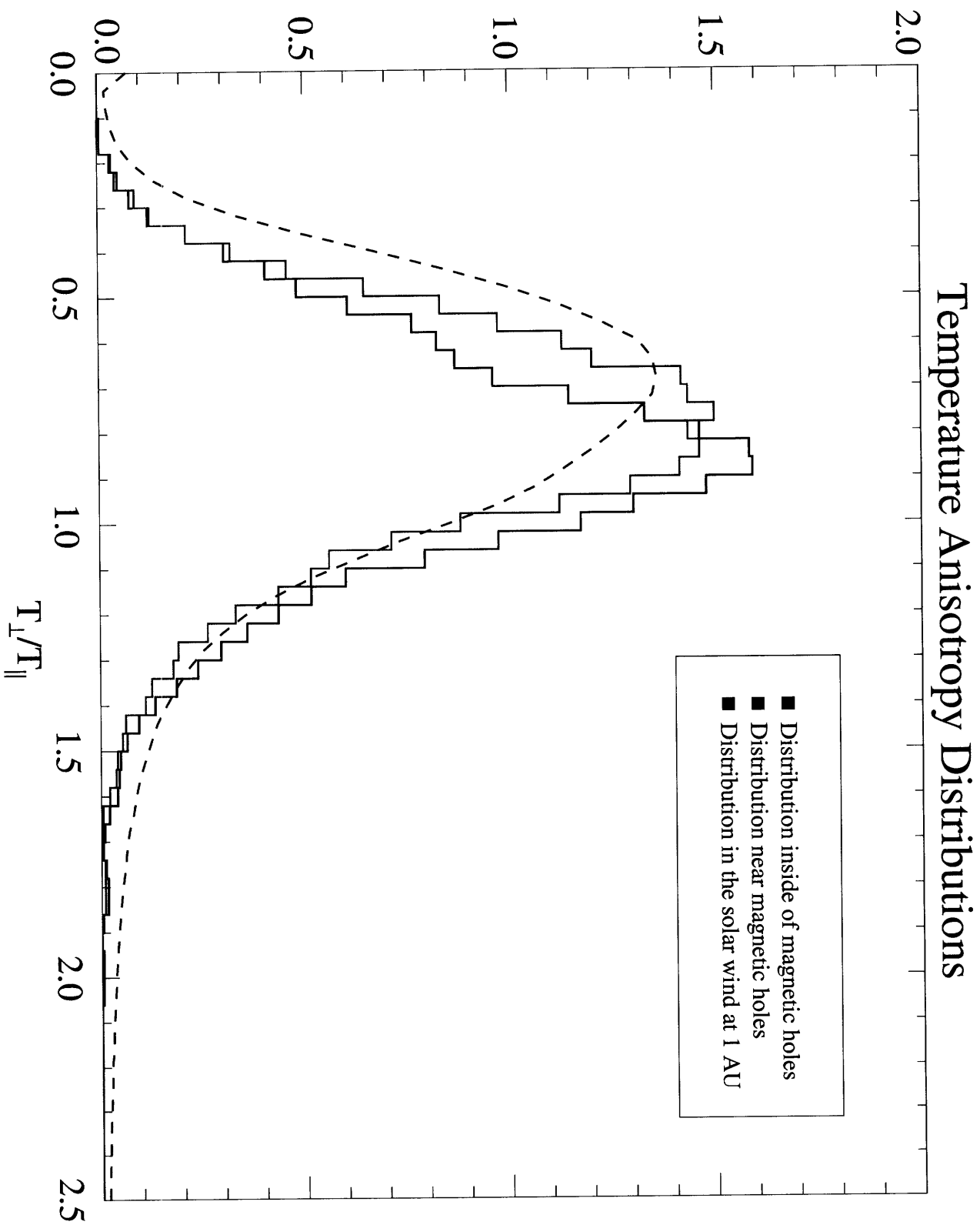


Figure 12

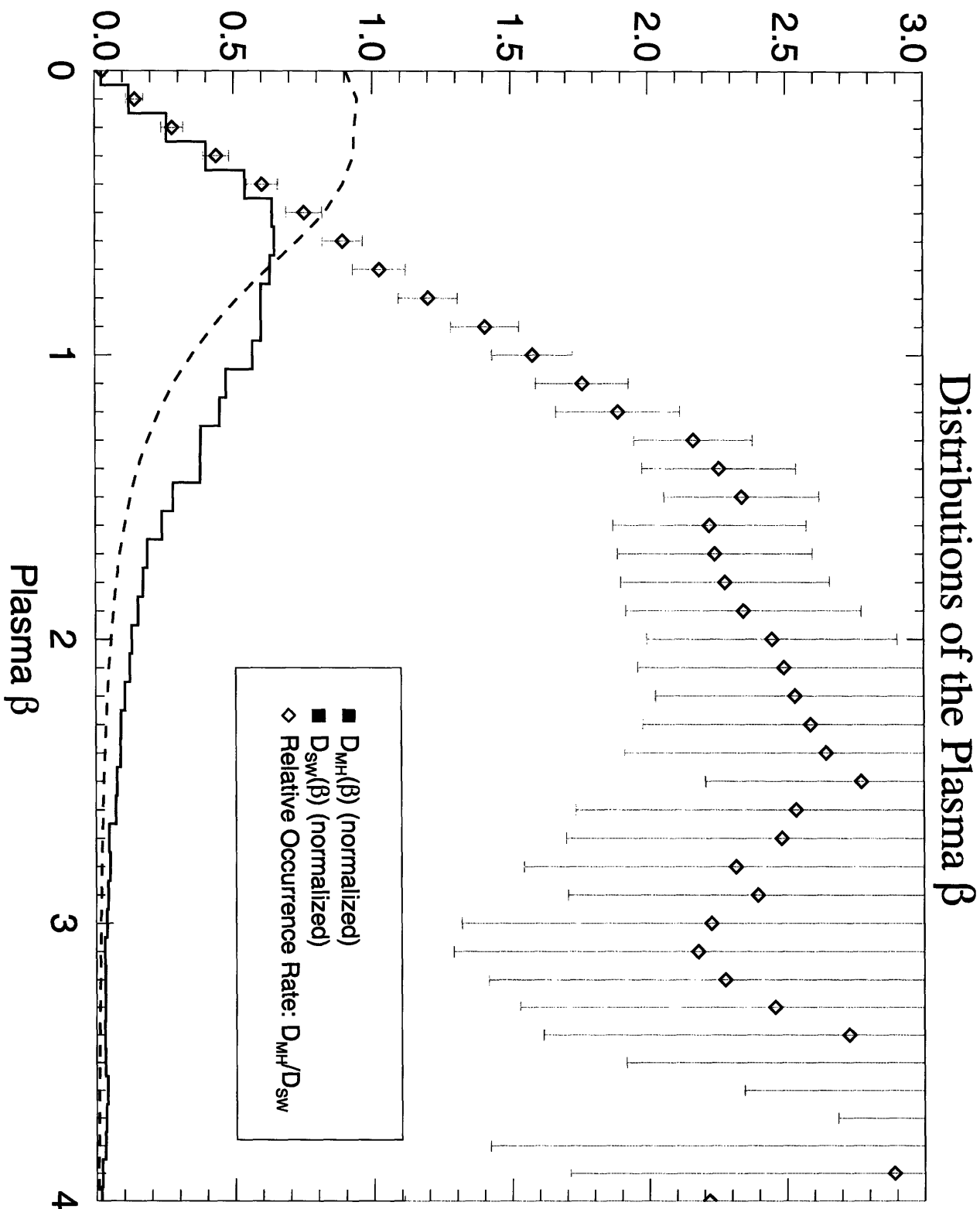


Figure 13

Hole Occurrences Relative to the Mirror Instability Threshold

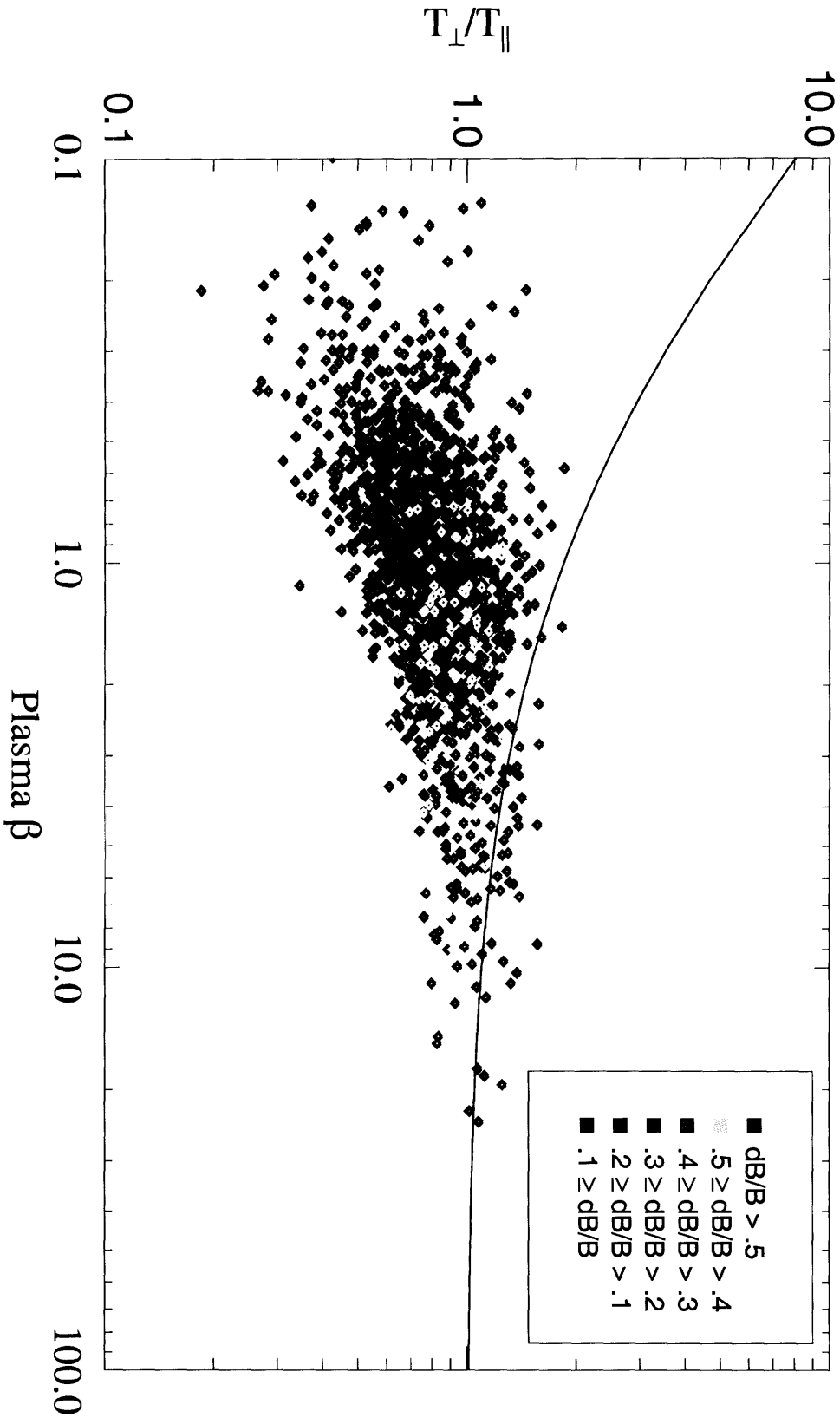


Figure 14

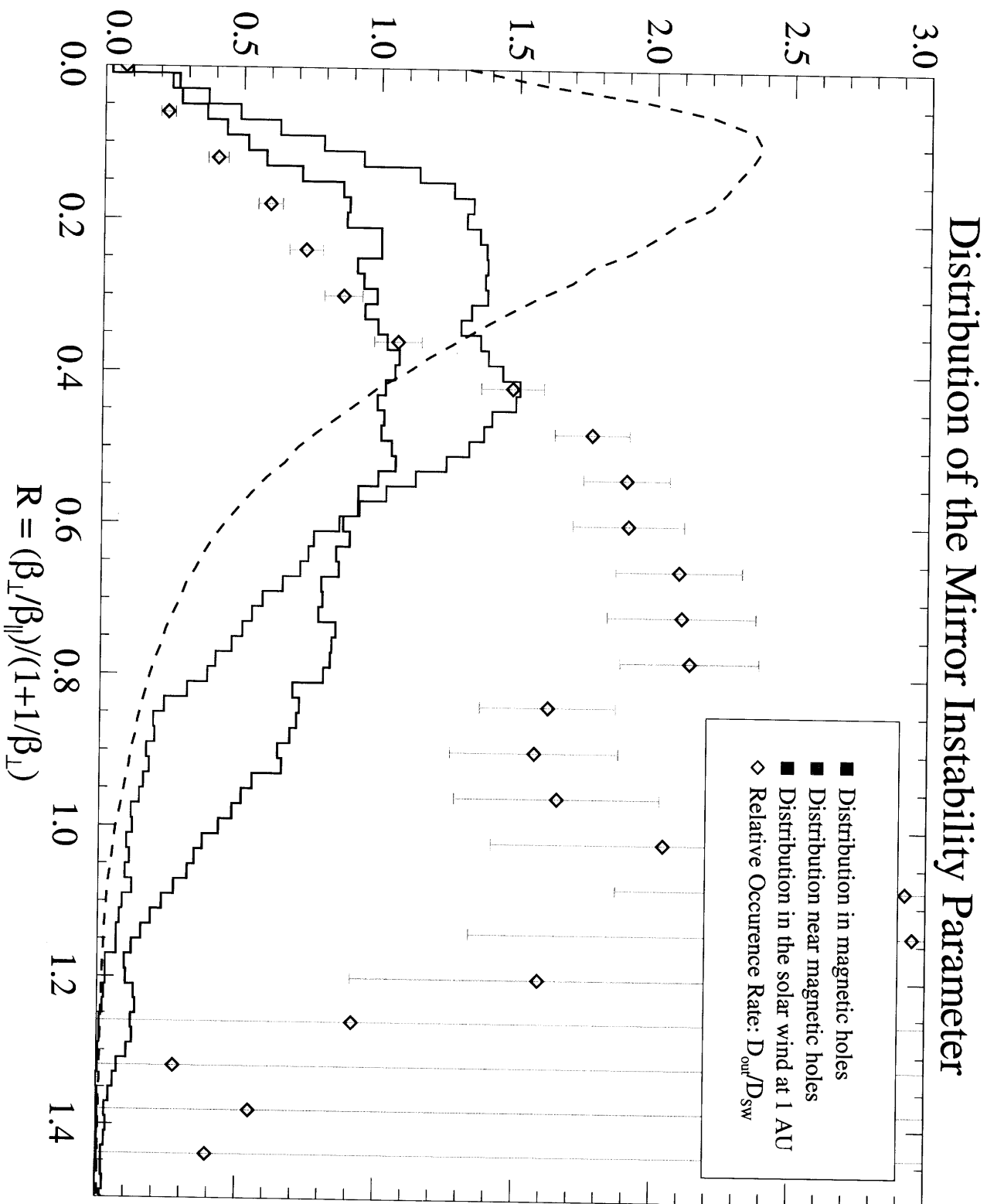


Figure 15